


Future 3D Additive Manufacturing
The 3DMM20 Conference



**3D Nano- and
Micro-Manufacturing:
Technology and
Technical Application**

**REGISTER
NOW!**

April 3 – 8, 2022 | Schöntal Monastery, Germany

Emission Manipulation by DNA Origami-Assisted Plasmonic Nanoantennas

Ayşe Tuğça Mina Yeşilyurt* and Jer-Shing Huang*

Plasmonic nanoantennas mediate far and near optical fields and confine the light to subwavelength dimensions. The spatial organization of nanoantenna elements is critical as it affects the interelement coupling and determines the resultant antenna mode. To couple quantum emitters to optical antennas, high precision on the order of a few nm with respect to the antenna is necessary. As an emerging nanofabrication technique, DNA origami has proven itself to be a robust nanobreadboard to obtain sub-5 nm positioning precision for a diverse range of materials. Eliminating the need for expensive state-of-the-art top-down fabrication facilities, DNA origami enables cost-efficient implementation of nanoscale architectures, including novel nanoantennas. The ability of DNA origami to deterministically position single quantum emitters into nanoscale hotspots further boosts the efficiency of light–matter interaction controlled via optical antennas. This review recapitulates the recent progress in plasmonic nanoantennas assisted by DNA origami and focuses on their various configurations. How those nanoantennas act on the emission and absorption properties of quantum emitters positioned in the hotspots is explicitly discussed. In the end, open challenges are outlined and future possibilities lying ahead are pointed out for this powerful triad of biotechnology, nanooptics, and photophysics.

1. Introduction

Antennas have stitched up far-flung parts of the globe and connected it to deep space and even provided us with information about the macro cosmos.^[1] In radio-frequency (RF) and microwave regimes, antennas' working wavelength is proportional to their physical size because in this spectral regime metals can be considered as perfect conductors.^[2] Shrinking the size of antennas to hundreds of nanometers would intuitively bring the working wavelength to the visible range.^[3] Compared to antennas in the RF and microwave regime, the main challenges for the realization of optical antennas lie in the nanofabrication, material properties as well as the control and manipulation of the excitation sources. Due to the ultrahigh working frequency, the functionality of optical antennas also expands from wireless communication to light–matter interaction. With the development of modern nanofabrication and detection technologies, ever smaller structures with exceptional

optical characteristics are assembled. Optical antennas made up of plasmonic nanoparticles are one of those constructs that can help overcome the size mismatch between matter and light waves in the topical regime and provide us a powerful tool for controlling and enhancing light–matter interaction.^[2,4–6]

Surface plasmon polaritons (SPPs) are coherent oscillations of the conduction electrons at the metal/dielectric boundary.^[7] Localized surface plasmons (LSPs) are confined SPPs on a plasmonic cavity, such as a noble metal nanoparticle in a dielectric medium. By changing the material, size, shape, and environment, the LSP resonance of the nanoparticle can be tuned. The tuned LSP enhances the polarizability of the nanoparticle at specific frequencies from ultraviolet to the near-infrared range, leading to peculiar optical properties that are distinctive from their bulk counterparts.^[8,9] When nanoparticles are arranged in specific configurations in space, LSPs couple and create more sophisticated, confined, and enhanced electromagnetic fields between and around them.^[10,11] These phenomena stem from the collective response of the nanoparticle architecture and are highly dependent on the selected material, the relative positioning of and the distance between the nanostructure components.^[12]


To describe the properties of optical antennas, the well-established RF antenna theories can be applied to a certain extent.^[13–16]

A. T. M. Yeşilyurt, J.-S. Huang
Leibniz Institute of Photonic Technology
Albert-Einstein-Straße 9, 07745 Jena, Germany
E-mail: mina.yesilyurt@leibniz-ipht.de; jer-shing.huang@leibniz-ipht.de

J.-S. Huang
Institute of Physical Chemistry and Abbe Center of Photonics
Friedrich-Schiller-Universität Jena
07743 Jena, Germany

J.-S. Huang
Research Center for Applied Sciences
Academia Sinica
Taipei 11529, Taiwan

J.-S. Huang
Department of Electrophysics
National Yang Ming Chiao Tung University
Hsinchu 30010, Taiwan

 The ORCID identification number(s) for the author(s) of this article can be found under <https://doi.org/10.1002/adom.202100848>.

© 2021 The Authors. Advanced Optical Materials published by Wiley-VCH GmbH. This is an open access article under the terms of the Creative Commons Attribution-NonCommercial-NoDerivs License, which permits use and distribution in any medium, provided the original work is properly cited, the use is non-commercial and no modifications or adaptations are made.

DOI: 10.1002/adom.202100848

However, the same design principles cannot be directly executed at optical frequencies since the material properties in the visible regime are significantly different from those in the RF or microwave regime.^[2] For instance, ubiquitously used metals that are very good conductors at RF become very lossy at the visible spectrum and field penetration depth that is comparable to dimensions of the antenna affects the effective wavelength of the plasmonic current and thus the antenna design and the emission properties.^[2,17,18] Furthermore, the operation of plasmonic nanoantennas goes beyond the transmission and reception of optical signals in wireless or on-chip communication networks.^[19] Plasmonic nanoantennas also offer the opportunity to enhance and control light–matter interaction and serve as building blocks of artificial metamaterials and metasurfaces.^[20] Plasmonic nanoantennas can be used to generate hot electrons^[21] or current^[22] and find applications in photochemistry,^[23] energy harvesting devices,^[24] and photon detectors.^[25] Field enhancement in the hotspot near nanoparticle surfaces is used to enhance nonlinear effects^[26] such as second harmonic,^[27,28] third harmonic signal,^[29] coherent anti-Stokes Raman scattering,^[30] and four-wave mixing.^[31] Likewise, if a plasmonic nanoantenna is combined with a gain material and their modes overlap spatially and spectrally, plasmonic lasing can be achieved.^[32–34] The tightly confined electromagnetic field in the gap with a size comparable to donor–acceptor distance is also utilized to enhance Förster resonance energy transfer efficiency by overcoming the nonradiative loss.^[35,36] Moreover, plasmonic nanoantennas can be engineered to provide directionality for spectroscopic analysis,^[37,38] sensing,^[39] and color routing for far-field^[40] and near-field light sources.^[41]

One of the most versatile plasmonic nanoantennas is a dimer consisting of two plasmonic nanoparticles of various geometries. The confined electromagnetic field in the gap of the dimer provides enhanced field intensity and localized density of optical states (LDOS).^[6] Therefore, plasmonic hotspots are commonly utilized to modify the emission of quantum emitters. If the coupling of the emitter to the antenna is efficient enough, the excited emitter relaxes by giving the energy into the efficient decay channels provided by the nanoantenna. Consequently, the observed emission property of the quantum emitter is highly modulated by the antenna. This provides a useful route to tailor the intensity, efficiency, spectrum, phase, polarization state, and direction of the emission from a quantum emitter. The effect of an optical antenna on these properties has a strong dependency on the spatial configuration of antenna elements and the emitter. Shape, size, and the distance between antenna components all influence the antenna mode. With the understanding of the resonance of individual elements and the coupling between them, optimal designs of nanoantennas can be found and verified with modern computational technology. However, the fabrication of the designed antennas and the deterministic incorporation of the emitters to the antenna are still challenging. The choice of nanofabrication method plays a determinant role in obtaining the desired structures and optical responses.

Nanoantennas, often, are fabricated by top-down methods such as electron-beam lithography (EBL) and focused ion-beam milling (FIB).^[2] EBL and FIB are widely used and very powerful nanofabrication techniques. However, they have

very low throughput and are limited to sub-10 nm alignment accuracy. This makes it difficult to achieve fine structures with sub-10 nm resolution.^[42] Besides, metals fabricated with top-down methods are typically polycrystalline with rough surfaces of grain size between 10 and 30 nm.^[43] Material inhomogeneity results in unwanted scattering and damping of surface plasmons that can greatly diminish the antenna performance.^[44] Building hybrid structures with top-down methods by incorporating different materials can be achieved in multiple steps^[45] or by selective chemical functionalization^[46] at the expense of time. Moreover, top-down methods require expensive state-of-the-art facilities and vacuum conditions and are typically lack scalability. Employing bottom-up approaches or combining top-down with bottom-up approaches provides effective solutions to address these issues.

DNA origami, which is considered to be a bridge between molecular self-assembly^[47] and conventional microfabrication techniques,^[48,49] allows to overcome these limitations and produce better performing plasmonic nanostructures. DNA origami is a bottom-up fabrication method to create platforms that support the building of complex, hierarchical, and hybrid structures.^[50–60] A DNA origami nanobreadboard is obtained by folding a long single-stranded DNA (scaffold) of a known sequence by hundreds of short oligonucleotides called staple strands, each one corresponding to a unique location in the scaffold.^[50] DNA origami is a tremendously addressable platform due to the Watson–Crick base pairing nature of the DNA and the availability of the sequence information of scaffold and staple strands. In plasmonic applications, gold and silver nanoparticles are incorporated into DNA origami by complementary strand hybridization. The metallic surfaces are coated with a certain length of staple strands that have exact complements, i.e., anchors, on the origami at desired locations.^[61–66] The distance between two nucleotides in the most ubiquitous DNA type-B is 0.34 nm.^[52] It has been shown that fluorescence molecules can be displaced in the subnanometer scale on DNA origami.^[67] However, this cannot be directly translated into positioning accuracy as it is affected by the length and flexibility of the anchoring and coating staples. The spatial resolution between the two DNA-linked nanomaterials on DNA origami is determined by the feature size of the origami, i.e., the length of the staple strand that the modifications are attached to, which is around 5 nm.^[68] Self-assembled monocrystalline metallic NPs,^[69–71] fluorescence molecules,^[72–74] semiconductor nanocrystals,^[74] nanodiamonds,^[75] and proteins^[76] are some of the materials that can be combined in the same one-pot experiment to produce billions of identical copies of the desired hybrid DNA-assisted nanostructures.^[77] In contrast to top-down methods that are inherently planar, DNA origami offers the possibility to create complex 3D nanostructures with almost any conceivable geometry. All in all, DNA origami serves as a precise, scalable, time-efficient, and relatively cheap platform to fabricate functional nanostructures, including metamolecules,^[74,78–82] plasmonic lenses,^[76,83] waveguides,^[75,84] and chiral nanostructures^[79,80,85–87] for applications in energy transfer schemes,^[36,88–90] super-resolution microscopy,^[91] and plasmon-enhanced circular dichroism.^[92] Another advantage of using DNA origami is that it enables the dynamic control of optical properties of as-built nanostructures. This can be achieved by

applying external stimuli such as changing the temperature,^[93] irradiation with light,^[94] or adding staple strands^[80,87,95,96] to cause a conformational change in the hybrid structure or forcing the walker to actively change its spatial coordinates on the origami frame.^[97,98] There have been many reviews on origami design, synthesis, and functionalization^[51,99,100] and how DNA origami is used to construct complex nanostructures.^[53–57] During the preparation of this manuscript, reviews on DNA origami-assisted nanostructures for sensing^[59] and spectroscopy^[60] have also been just published.

In this review, we summarize the recent and pioneering works in DNA origami-assisted plasmonic nanoantennas and elaborate on how these antennas manipulate the emission and absorption properties of quantum emitters precisely positioned in their hotspots.

2. DNA Origami-Assisted Plasmonic Nanoantennas

Design parameters such as material, number, size, and geometry of antenna components and their relative spatial positions determine the resonance and the radiation characteristics of a plasmonic nanoantenna. Interparticle distance between the elements of an antenna is particularly critical as it determines the resonance of the antenna and the electromagnetic environment experienced by the quantum emitter placed in the hotspot. DNA origami provides nanometer-scale localization accuracy and addressability. Hence, DNA origami enables the fabrication of plasmonic nanoantennas with small gaps and immobilization of single quantum entities in the hotspots. DNA origami-assisted plasmonic nanoantennas provide extraordinary spontaneous emission rate enhancement,^[101–110] strong coupling,^[111–114] Raman signal enhancement,^[115–125] and rather humble control of emission directionality^[126] and emission polarization^[127] of single emitters.

2.1. Fluorescence Intensity and Radiative Decay Rate Enhancement

Purcell in his renowned work showed that the same emitter in free space and a cavity has different emission properties due to the different photonic environments it is exposed to.^[128] Whether the cavity is a single nanoparticle or a plasmonic dimer gap, the total LDOS experienced by the emitter is altered by the presence of the antenna. As a starting point, the quantum emitter and the antenna can be thought of as two separate resonators. When the coupling between them is “weak,” both objects are treated as isolated resonators and the emission frequency of the emitter is not significantly affected by the antenna. In this weak coupling regime, the spontaneous emission property of the emitter can be modified by the antenna due to the additional channels provided by the antenna. However, when the energy exchange between them is faster than the energy dissipation, the emitter and the plasmonic cavity are in the strong coupling regime, where the electronic states of the emitter and the photonic states of the antenna hybridize.^[129] The electromagnetic energy between the emitter and antenna

is coherently and reversibly interchanged between the two components of the new hybrid object.

In the weak coupling regime, depending on the spatial location of the emitter and the design of the antenna, the excited emitter relaxes into the additional radiative and nonradiative decay channels provided by the antenna.^[130,131] The radiative and nonradiative channels together determine the overall emission rate. If the emitter couples more effectively to the bright resonance modes than the dark ones, the antenna serves as a mediator to help emit the local energy of the emitter to the far field, leading to enhanced emission brightness. The additional decay channels provided by the nanoantennas, no matter radiative or nonradiative, reduce the emission lifetime.^[132] The enhancement in the emission brightness depends, however, on the intrinsic quantum yield (QY_o) of the quantum emitter ($QY_o = \gamma_{r,o}/(\gamma_{r,o} + \gamma_{nr,o})$, $\gamma_{r,o}$: radiative and $\gamma_{nr,o}$: nonradiative decay rate in the absence of a plasmonic antenna). For a high QY_o emitter, since the emitter already works in saturation, an increase in radiative decay does not necessitate an increase in brightness but shortens the lifetime τ ($\tau = (\gamma_r + \gamma_{nr})^{-1}$, γ_r : radiative and γ_{nr} : nonradiative decay rate of an emitter coupled to a plasmonic antenna). Whereas, for an inefficient emitter, an increase in γ_r can significantly increase its brightness. On the other hand, when the emitter couples more effectively into the dark modes than the bright ones, the nonradiative decay channel dominates. In this case, the subradiant resonant modes are excited and the energy mainly dissipates into heat.^[133] Although dark modes cannot be directly excited by far-field illumination, they can still be excited if they couple to bright modes or near-field light sources, such as quantum emitters. This allows dark modes to provide enhanced optical near fields upon far-field illumination^[134] and contribute to the reduction of emission lifetime. Altogether, an increase in the total LDOS reduces the excited state lifetime of a quantum emitter. The spontaneous emission rate increases if the relaxation is dominated by the bright modes. Typically, the emission lifetime of a quantum emitter ranges between a few to tens of nanoseconds. When coupled to a plasmonic nanoantenna, the emission lifetime can be reduced to picosecond regime, rendering the emitter a fast, bright, and controllable photon source.^[130,135] Organic dyes,^[136,137] semiconductor nanocrystals,^[138] and nitrogen-vacancy centers^[139] are some of the commonly used emitters in this regard.

So far, one challenging task in plasmonic nanoantenna fabrication is the precise positioning of single quantum emitters in the hotspots. Most of the quantum emitters mentioned previously can be chemically functionalized with single strands of known DNA sequences that have a complementary strand protruding from the DNA origami. The protrusion locations are determined by the necessities of the antenna design. Placing a single emitter in the vicinity of a nanoantenna can be achieved easily in a single step with DNA origami, whereas it takes multiple steps and with sub-10 nm accuracy by top-down methods.^[140] Moreover, DNA origami’s design ability and nanoscale positioning accuracy allows for the realization of sub-5 nm gaps with fairly high repeatability and product yield.

The first deterministic demonstration of placing a single molecule at a hotspot of a dimer antenna using DNA origami was achieved by Acuna et al.^[101] The pillar origami used had

a length of 220 nm, a 15 nm diameter made up of a 12-helix bundle, and three additional six-helix bundles on the base with a 30 nm base diameter. The base contained biotin-modified strands to immobilize the pillar upright when neutravidin-coated substrates were used. A single ATTO647N dye molecule was incorporated at the half-height of the pillar, where 80 and 100 nm AuNP dimers were also immobilized separately to form dipole antennas with a gap of 23 nm, as shown in **Figure 1a**. Fluorescence transients of the fluorophore incorporated into an antenna with 80 nm AuNP dimer and a single AuNP were compared to that of a single dye molecule without any AuNP. The typical lifetime of an ATTO647N dye molecule is 3.8 ns. A decrease in the lifetime from 3.8 ns to 1.17 for a monomer and to 0.22 ns for a dimer was observed as given in the lower panel of Figure 1a. Intensity profiles of different spots on fluorescence images were sorted and histograms were made for statistical analysis of fluorescence enhancement (FE). For 100 nm dimers, the average brightness enhancement was 28 and some dimers exhibited an FE of more than 100. The same group, later, showed that it is possible to obtain even higher enhancement from a single fluorescing molecule with a modified pillar origami.^[102] The total height of the pillar was reduced to 125 nm with the main shaft of a 12-helix bundle. ATTO647N dye molecule was incorporated to the last 29 nm of the pillar, where the pillar thickness was reduced to six-helix bundles. Two 100 nm AuNPs were immobilized around the fluorophore with a zipper configured complementary strand hybridization. Shear and zipper configurations are two ways of hybridizing the capturing staples with their complementary DNA sequences on the nanoentity surface that is decorating the origami. Shear configuration is formed when 5' (3') of capturing strand corresponds to 3' (5') of the complementary staple making the duplex normal to both surfaces. Thus, the distance between the origami and the nanoentity is determined by the length of the capturing strand. Zipper configuration is formed when 5' (3') of capturing strand

corresponds to 5' (3') of the complementary staple and the duplex becomes tangential to both surfaces, eventually minimizing the distance between them. Therefore, by utilizing the zipper arrangement Puchkova et al.^[102] reduced the gap size to 12–17 nm. The incident field was also oriented along the dimer axis to excite the longitudinal mode of the antenna to obtain the maximum field enhancement in the hotspot. As mentioned earlier, the fluorescence intensity enhancement has a strong dependency on the QY_0 of the emitter in the hotspot. In this work, the product of the overall observed FE and QY_0 was taken as the figure of merit for FE since it reflects best the coupling between the nanoantenna and the emitter and liberates the enhancement from its dependency on the intrinsic efficiency. Accordingly, they obtained the highest FE figure of merit of 306 for ATTO647N. Since Atto647N is a high intrinsic quantum yield emitter ($QY_0 = 0.65$) to obtain even higher FE, $NiCl_2$ was used as a quencher to decrease its QY_0 and a 5468-fold FE was recorded. Finally, to enable the detection of single molecules in highly concentrated samples, ATTO647N dye-labeled oligonucleotides were added to antennas with hotspots only having the capturing strands. In the case of no quencher in the solution, it was possible to detect the fluorescence of a single Atto647N dye molecule when the dye concentration was 5×10^{-6} M. When the dyes were quenched with $NiCl_2$, 25×10^{-6} M was the highest reported concentration at which the fluorescence from a single dye was still detectable in such a concentrated background of fluorophores.^[102] At the same time, Zhang et al. reported an FE of 470-fold at a single-molecule level from Atto-655 dye molecules that randomly diffused into the gap between two gold nanorods (AuNR) assembled on a rectangular DNA origami of size $43 \text{ nm} \times 11 \text{ nm}$.^[103] After surface immobilization, AuNR dimers were embedded in a flow cell and the concentration of fluorophores was adjusted in a way that, on average, 7.5 molecules were found in the laser focal volume. Temporally separated fluorescence bursts from dye molecules that diffused into

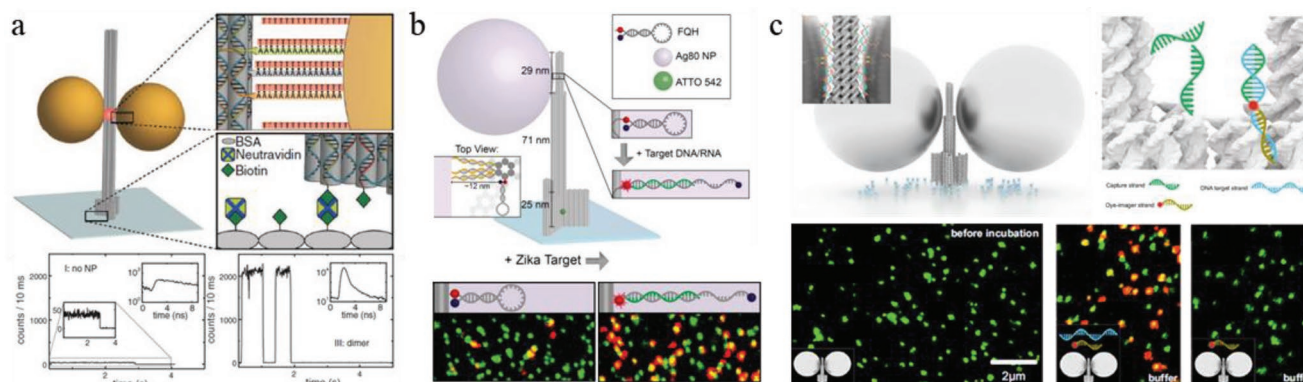


Figure 1. Dimer antennas assembled by pillar DNA origamis. a) Upper panel: 80 nm AuNP dimer antenna with a single ATTO647N dye molecule at the 23 nm wide hotspot. Pillar is immobilized on neutravidin functionalized glass cover by biotin extensions on the origami. Lower panels: Intensity transients and their fluorescence decays of the dye without (left) and with (right) nanoparticles. Reproduced with permission.^[101] Copyright 2012, The American Association for the Advancement of Science. b) Upper panel: Upgraded pillar origami decorated with a single silver nanoparticle (AgNP) of 80 nm and a schematic of the DNA-based fluorescence-quenching hairpin to detect the Zika-specific DNA. Lower panel: Fluorescence images of surface-immobilized pillar antennas before and after the addition of target Zika-specific DNA after 18 h incubation. Adapted with permission.^[104] Copyright 2017, American Chemical Society. c) Top left: Schematic of NanoAntennas with Cleared HOTSpots (NACHOS) with two 100 nm AgNP. Top right: Three capture strands at the hotspot to detect target DNA sequence with imager strand. Bottom panel: Fluorescence images before (left), after addition of target DNA and imager strands (middle), and after addition of only the imager strands without the target (right). Reproduced with permission.^[109] Copyright 2021, Springer Nature.

the hotspot were collected and the corresponding FEs were calculated for different separations between AuNRs. The gap sizes varied from 6.1 to 26 nm and the highest FE was found to be 470 for the 6.1 nm gap. Increasing the separation to 26 nm decreased the FE to 120-fold, which was close to that of a single AuNR. Tinnefeld group, later, decorated the pillar origami with a single 80 nm silver nanoparticle (AgNP) to detect Zika-specific DNA with single-molecule sensitivity^[104] and used it also as a fluorogenic nucleic acid hybridization probe.^[105] In both studies, a fluorescence-quenching hairpin (FQH) was used. For the former, FQH that was complementary to Zika's envelope protein was embedded in the pillar next to the AgNP as shown in Figure 1b. When Zika-specific target DNA was in the environment, FQH opened and separated the fluorophore from its quencher and up to 60-fold FE was obtained. Steric effects of negatively charged nanoparticles, capturing strands and origami pillar hindered the immobilization of a second AgNP and resulted in an average FE of 7.3. The same group later achieved immobilization of two 80 nm AgNPs in the pillar and obtained low absorption and high scattering cross-section in the green and blue parts of the visible spectrum that could not be achieved with gold.^[106] Alexa488, Atto542, and Atto647N dye molecules, all with high intrinsic quantum yield and photostability, were individually put in the hotspot of 12 nm between AgNPs and their fluorescence transients were recorded. The same design and experiments were performed with 100 nm AuNP dimers to compare the performances of silver and gold antennas for different wavelengths. For antennas built with AgNPs, maximum FE of 183, 207, and 400 were measured in the blue, green, and red spectral ranges. For antennas using AuNPs, maximum FE values were 3, 17, and 430, respectively. These results confirmed that silver antennas, indeed, could yield a broadband FE in the entire visible spectrum. Although AgNPs increased the photostability of Alexa488, it was reported that silver oxidation hampered its radiative decay rate enhancement.^[107]

Later, Kaminska et al. used the pillar origamis with 100 nm AuNP and 80 nm AgNP dimers to overcome the size mismatch between light and a light-harvesting molecule peridinin-chlorophyll α -protein (PCP) complex.^[108] PCP was incorporated into the pillar by biotin-streptavidin conjugation in the dimer gap of ≈ 12 nm. Peridinin molecule was excited with 532 nm laser and maximum FE of 145 and 120 were acquired from gold and silver antennas, respectively. When a 640 nm laser was used to excite the chlorophyll α molecule, 526-fold from AuNP and 250-fold FE from AgNP dimers were obtained. These values were the highest recorded enhancements for PCP. Trofymchuk et al. recently showed that by utilizing the fluorescence amplification provided by the DNA origami-assembled NanoAntennas with Cleared HOTspots (NACHOS), single-molecule detection with low-cost, low-numerical aperture optics is possible.^[109] Two 83 nm high pillar DNA origamis were attached to form an estimated gap of 12 nm. Two 100 nm AgNPs were immobilized on both sides of the gap and three capturing strands were protruding in the hotspot to capture the target DNA as shown in the upper panel of Figure 1c. The target was 34 nucleotides long, genetic code that is used in the diagnosis of the antibiotic-resistant bacteria *Klebsiella pneumoniae* infection. The first half of the target DNA sequence complemented the capture strands each being 17 nucleotides long. The remaining half

of the target DNA sequence complemented the Alexa Fluor 647 dye-labeled imager strand. Once the target bound to the imager strand, fluorophore was immobilized in the hotspot and underwent an enhancement in the emission. Therefore, the increased fluorescence of the dye reported the existence of the target molecule in the environment. When a single target was immobilized in the hotspot in buffer solution, an FE up to 461 with an average of 89 ± 7 was observed. Since there were three capture strands in each hotspot, they identified the antennas having a single target by counting the photobleaching steps in the time trajectory of fluorescence intensity. 60% of the dimer antennas contained a single target. NACHOS were also used in target spiked human blood serum, where a variety of other biological molecules in high concentrations were present. In the human blood, an FE of a maximum 457 with an average of 70 ± 4 was obtained. Designs like NACHOS bring portable smartphone microscopes a step closer to on-site detection and diagnostic applications.

Until now, we discuss the coupling of quantum emitters with antennas weakly and efficiently. To transit to the strong coupling regime, intense field localization at the quantum emitter's position should be ensured. The electric field is tightly confined in plasmonic hotspots and scales with the actual volume of the hotspot. Smaller plasmonic gaps facilitate stronger cavity-emitter coupling strength.^[141] Also, emitters with high dipole moments or in high concentrations enhance the coupling strength. For strong coupling, DNA origami offers a unique opportunity to achieve ultrasmall gaps between plasmonic nanoparticles. Roller et al. used a two-layered rectangular DNA origami sheet to fabricate a well-controlled plasmonic gap from a gold dimer and reported a strong coupling with a layer of cyanine-based dye J-aggregate.^[111] AuNPs of varying diameters from 30 to 60 nm were placed on opposing sides of the origami with a fixed separation of 5 nm. They found that the longitudinal mode of a 40 nm AuNP dimer matches best with the J-aggregate's resonance frequency. From split peaks on the scattering spectra of dimers, a fitted Rabi splitting of ≈ 150 meV was calculated and it is illustrated in Figure 2a. The authors also calculated the coupling constant for each dimer and found that there is an inverse relationship between the nanoparticle radius and the coupling constant. Later on, the first near-field mapping of a plasmonic cavity operating in a weak-to-strong coupling regime by a single-molecule was demonstrated by Chikkaraddy et al.^[112] A rectangular two-layer plate origami was used to obtain a nanoparticle-on-mirror structure as shown in Figure 2b. The gap size of 4.3 ± 0.3 nm was determined by the thickness of the origami sheet. A Cy5 dye molecule was placed in the middle of the rectangle and was surrounded by six capture strands to immobilize an 80 nm AuNP on the upper side of the origami. From the bottom side, origami was already placed on a gold film. Dye was placed in between two plasmonic structures constituting the cavity. A mean Rabi splitting of 80 meV was obtained for more than 200 structures. Without undergoing quenching, the dye experienced an FE of more than 1000. By deterministically changing the lateral position of the dye in the cavity, electromagnetic modes of the cavity were mapped at 1.5 nm spatial resolution. Since controlling the orientation of the transition dipole in the experiment was extremely challenging, the authors only estimated the most probable dipole

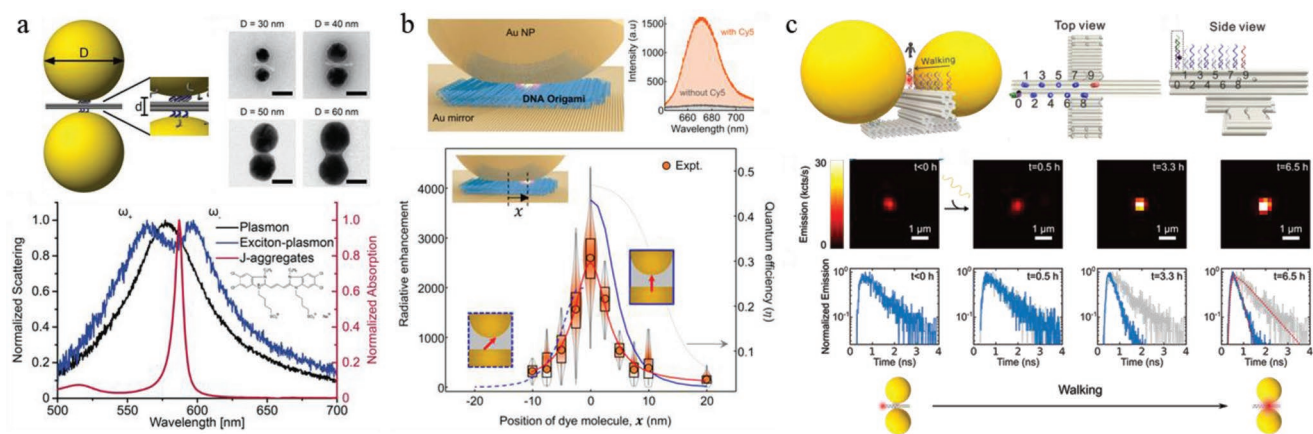


Figure 2. Hybrid nanostructures in the strong coupling regime and the DNA walker construct. a) Top: Schematic of the gold dimer with a fixed gap distance of ≈ 5 nm. TEM images of dimers constructed with 30, 40, 50, and 60 nm AuNPs. Bottom: Peak splitting of normalized scattering spectrum of the strongly coupled 40 nm AuNP dimer and J-aggregate. Adapted with permission.^[111] Copyright 2016, American Chemical Society. b) Top left: An 80 nm AuNP on rectangular origami sheet hosting a single Cy5 molecule in its center on a gold film. Top right: Optical emission from nanoparticle-on-mirror with (red) and without (gray) Cy5 dye molecule in the DNA origami. Bottom panel: Mapping the radiative LDOS by changing the lateral position of Cy5 in the gap. Adapted with permission.^[112] Copyright 2017, American Chemical Society. c) Top panel: Schematics of the walking platform ending at the hotspot of 60 nm AuNP dimer. Fluorescence maps of a single walking device taken at different instants of 6.5 h walk (middle panel) and the respective fluorescence lifetime of ATTO647N dye molecule as it progresses towards the hotspot (lower panel). Adapted with permission.^[110] Copyright 2019, American Chemical Society.

orientation by comparing the simulated results obtained under 90° (normal to metal film) and 45° dipole orientation with the experimental results. The best fit of the dipole orientation was found to be $65^\circ \pm 15^\circ$. This work demonstrates that, by placing fluorophores in ultrasmall gaps, enormous emission enhancements can be obtained without quenching. Subsequently, the same group reported the interaction of a single Atto647 dye molecule sitting at the plasmonic gap of the same nanoparticle-on-mirror structure with ultrafast pulses at room temperature in ambient conditions.^[113] The plasmon resonance of the cavity did not match the absorption peak but instead, it matched the emission peak of the fluorophore. Therefore, the photoluminescence spectrum of the hybrid system exhibited split peaks with a Rabi splitting of 30 ± 5 meV. When the sample was excited with 120 fs laser, a significant lifetime reduction from 2.5 ± 0.2 to 0.3 ± 0.1 ns limited by the instrument response time was observed. Later, strong coupling with J-aggregates of 5,6-dichloro-2-[[5,6-dichloro-1-ethyl-3-(4-sulfobutyl)-benzimidazol-2-ylidene]-propenyl]-1-ethyl-3-(4-sulfobutyl)-benzimidazolium hydroxide inner salt (TDBC) with a chiral plasmonic nanocavity was reported by Ding and co-workers.^[114] Left- and right-handed chiral structures were made of two AuNRs ($40 \text{ nm} \times 10 \text{ nm}$) attached on the opposite sides of a rectangular origami ($90 \text{ nm} \times 60 \text{ nm} \times 2 \text{ nm}$) with a 90° angle to form an L-shape. These nanostructures support symmetric and antisymmetric resonance modes around the extinction peak of a single AuNR. To spectrally overlap the symmetric mode with the resonance of the TDBC J-aggregate, a thin shell of silver was grown on AuNRs and the TDBC was adsorbed on the surface of the core-shell nanorods. Circular dichroism spectra of the enantiomers showed the splitting of the symmetric mode. The Rabi splitting of the system was determined to be 205 and 199 meV for left- and right-handed chiral nanostructures, respectively.

2.1.1. Dynamically Tunable DNA Origami-Assisted Plasmonic Nanoantenna

Including the nanoparticle-on-mirror construct, all aforementioned nanoantennas were static. In other words, the placement of nanoparticles and fluorescing entities were predefined and once built they could not be changed. Chikkarady et al.^[112] built multiple static nanoparticle-on-mirrors, and in each batch, the emitter was positioned at a different location to map the LDOS of the gap. On the other hand, Xin et al. reported a dynamic origami system in which the position of the emitter was changed by applying an external stimulus and observed fluorescence lifetime decrease of and emission enhancement from a single emitter in real-time.^[110] The origami consisted of a bottom part and a platform to accommodate two 60 nm AuNPs with a nominal gap of 15 nm as displayed in Figure 2c. The walking platform was 10 nm in width with 10 RNA stators located in a zigzag fashion. The height of the platform was adjusted to be the same level as the hotspot of the dimer. DNAzyme, the walker carrying ATTO647N dye reporter molecule, was induced to walk with the addition of Mg^{2+} that catalyzed the cleavage of the stators with a step size of 5.2 nm. This burnt-bridge mechanism forced the walker to continue its unidirectional progression autonomously. According to numerical simulations, the maximum FE that could be achieved was 9. In the experiment, however, the maximum FE after 6.5 h of walking was only ≈ 4 . The steric forces in the gap might have prevented the fluorophore to enter exactly into the hotspot, therefore reduced the FE. From the numerical simulations, the gap size was determined to be 21 nm. The average lifetime reduction obtained from 24 devices was a factor of 3. Real-time control over the location of a reporter molecule has never been achieved in top-down methods and is only possible with tailor-made DNA origami platforms with careful control over the environmental conditions.

2.2. Absorption Enhancement and Surface-Enhanced Raman Scattering (SERS)

The wavelength of visible light (400–750 nm) is orders of magnitude bigger than the length scale of electronic confinement in molecules (sub to few nm). When the incident light field couples to plasmons, the excitation wavelength shrinks down and the field can be very tightly confined at the hotspots around the plasmonic nanoparticles. This helps to overcome the size mismatch between light and matter and has important consequences. First, as the field intensity increases, the excitation rate can be greatly enhanced. Second, higher-order multipolar and forbidden transitions might become accessible due to the modification of the symmetry and selection rules.^[142,143]

Absorption and scattering cross-sections of single molecules are typically around 10^{-25} and 10^{-30} cm², respectively.^[144] These infinitesimal values render the spectroscopic analysis of vibrations of single molecules very difficult. To increase the likelihood of obtaining a photon reporting a vibrational transition, high electric field enhancement provided by plasmonic structures has been used.^[145–148] Raman scattering enhanced by hotspots or rough surfaces of metal is named surface-enhanced Raman scattering. SERS offers high sensitivity and specificity to detect analytes at ultralow concentrations even down to the single-molecule level.^[149] SERS enhancement is proportional to the fourth power of the electric field at the molecule's position. Therefore placing a single molecule exactly at the hotspot is very important. To obtain more intense fields, gap sizes between 2 and 10 nm are used and typical enhancement factors of 10^5 – 10^6 are obtained.^[145–147] In addition to increased electromagnetic enhancement in the hotspot, the Raman signal undergoes an additional chemical enhancement due to the bond formed between the molecule and the metal if the molecules are in contact with the nanostructures.^[144,145,147]

The first demonstration of using DNA origami-assisted AuNPs as SERS substrates was achieved by Prinz et al.^[115] Two 5 nm AuNPs were immobilized on the triangular origami by complementary strand hybridization to form a dimer with a nominal gap of 25 nm. To obtain higher field enhancement in the hotspot, the gap size was shrunk by increasing the AuNP size to 25 nm with electroless gold deposition. A carboxytetramethylrhodamine (TAMRA) dye molecule was immobilized in the gap between AuNPs. The highest enhancement factor was obtained at 1650 cm⁻¹ from 17 dimers in the confocal detection area, each having a single TAMRA dye molecule. Pilo-pais et al. also used chemical deposition to obtain bigger nanoparticles and smaller interparticle distances to obtain higher field enhancements and more pronounced Raman signals.^[116] They decorated each corner of a rectangular origami with a 5 nm AuNP and grew them with the HQ SILVER to a final size of 50 nm. Then, 4-aminobenzenethiol dye molecules as the Raman reporters were deposited on the tetramers and more than a 100-fold enhancement per nanoparticle at 1075 cm⁻¹ was observed. About the same time, Thacker et al. obtained up to seven orders of magnitude enhancement of Raman signal from Rhodamine 6G dye molecules in a single DNA origami-assembled AuNP dimer structure.^[117] They designed a novel multilayer origami platform with two grooves to accommodate two 40 nm AuNPs and separated them with a ridge of double

helices, enabling the shortest controllable gap of 3.3 ± 1 nm as shown in Figure 3a. The excitation polarization-resolved scattering spectrum clearly showed a redshifted and enhanced resonance peak with polarization along the dimer axis, i.e., longitudinal mode of the antenna. This redshift is a signature of plasmon coupling between the two nanoparticles. As for the scattering with excitation polarization transverse to the dimer axis, the scattering spectrum was the same as that of a single 40 nm AuNP. Dimers immobilized on a gold-coated silicon wafer were covered with a monolayer of Rhodamine 6G. The number of molecules per gap was estimated to be 5. An enhancement factor of 10^5 – 10^7 was obtained depending on the orientation of the dimer axis with respect to the excitation field.

Similarly, Kühler et al. used a gold dimer to enhance the Raman signal of fluorophores in the hotspot of the antenna.^[118] Two 40 nm AuNPs were immobilized on both sides of a three-layer rectangular origami. The thickness of the DNA sheet, which determined the gap between the nanoparticles, was estimated to be 6 ± 1 nm. SYBR Gold nucleic acid gel stain was used as the Raman molecule that bound to double-stranded DNA constituting the origami. A mean SERS enhancement factor of 3.1×10^5 for the peak at 1365 cm⁻¹ was observed from an estimated number of 25 dye molecules in the hotspot. By decreasing the number of layers, the interparticle distance could have been reduced at the expense of structural rigidity. The flexibility of structure means more uncertainty in the gap size that is detrimental for higher Raman enhancement factors. Therefore, the same group, later on, reported a method to reduce the dimer separation down to 1–2 nm by thermally tuning the origami thickness and quantitatively showed Raman signal enhancement of a single molecule.^[119] Two 40 nm AuNPs were bound on both sides of a five-layer rectangular origami. Only the central rectangle was a full sheet, the remaining layers were frame structures. The middle layer enabled the site-specific binding of a single Cy3.5 dye molecule as a Raman reporter as displayed in Figure 3b. Upon laser irradiation, the gap size decreased since heating the origami shrinks its thickness uniformly. Rayleigh and Raman spectra of the dimers were measured before heating with laser and no peaks correlated to Cy3.5 molecule were observed. After 10 s of irradiation with 60 kW cm⁻² power density, a redshift of 26 nm in the scattering spectrum was observed, and the Raman peaks of Cy3.5 molecule started to emerge in the Raman spectrum. After the second heating step, a 30 nm redshift was observed and Raman peaks became even more pronounced as demonstrated in the right-most panel of Figure 3b. By using the Mie theory, gap sizes were calculated and it was found that gaps were reduced irreversibly from 3.3 to 1.9 nm after the first and from 1.9 to 1.3 nm after the second heating step.

At the same time, Prinz et al. demonstrated plasmonic SERS with sensitivity down to single-molecule level using DNA origami-assisted Au-Ag-core-shell nanoantennas.^[120] Two 60 nm AuNPs were captured from opposite ends of a triangular origami and an ≈ 10 nm thick silver shell was chemically grown on AuNPs leaving a smaller gap in between as illustrated in Figure 3c. Single TAMRA or Cy3 fluorophores were already embedded in the hotspot on the origami. Many dimer structures with a single dye molecule were measured, and for Cy3 at least six characteristic bands were observed to confirm

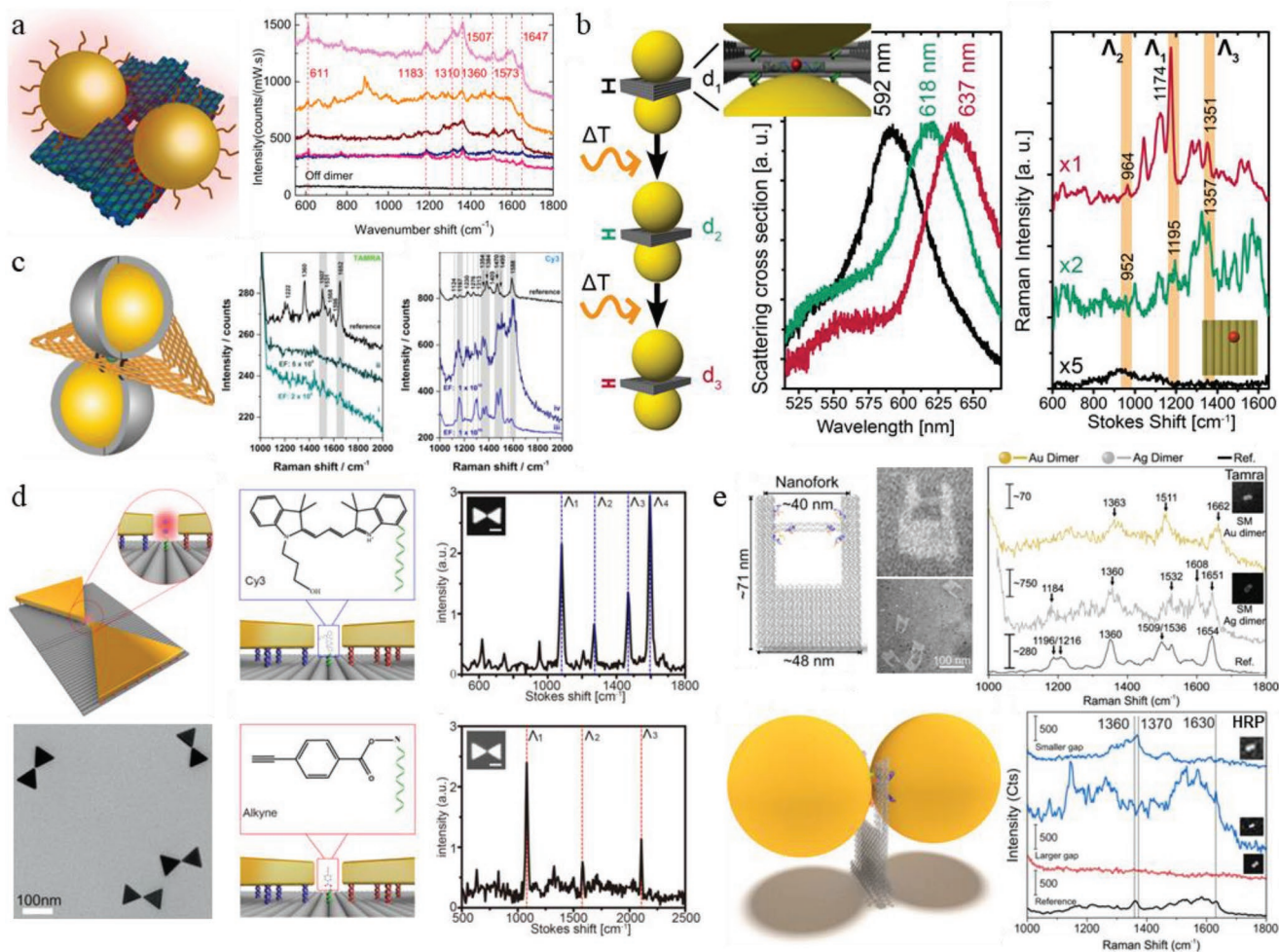


Figure 3. Dimer antennas for SERS. a) Left: Schematic of 40 nm AuNP dimer on the groovy origami with 3.3 ± 1 nm gap size. A monolayer of Rhodamine 6G covers the antenna and the hotspot. Right: SERS spectra of several dimer antennas. Dashed lines correspond to Rhodamine 6G peaks enhanced by the antenna. Reproduced with permission.^[117] Copyright 2014, Springer Nature. b) A schematic of a 40 nm AuNP dimer accommodated in a frame-like rectangular origami. Only one Cy3.5 molecule is immobilized in the hotspot by site-specific binding. With laser irradiation, gap size shrinks, scattering spectrum redshifts, and Raman bands become more pronounced. Adapted with permission.^[119] Copyright 2016, American Chemical Society. c) Left-most: Schematic of DNA origami-based Au-Ag-core-shell nanoantenna. Raman scattering spectrum of TAMRA (middle) and Cy3 (right) dye molecules fixed at the dimer hotspot on the triangular DNA origami. Reproduced with permission.^[120] Copyright 2016, The Royal Society of Chemistry. d) Top-left: Schematic of a bowtie nanoantenna made of gold nanoprisms with a side length of 80 nm. Bottom-left: TEM image of fabricated bowtie antennas. A single molecule can be captured by site-specific binding. Chemical structure and Raman scattering spectrum of Cy3 (top-middle and top-right panels) and a single alkyne (bottom-middle and bottom-right panels) are given. Reproduced with permission.^[123] Copyright 2018, John Wiley and Sons. e) Top-left: DNA origami nanofork design and TEM images. Bottom-left: Schematic of a DNA origami nanofork antenna (DONA) with 60 nm AuNPs. Top-right: Raman scattering spectra of TAMRA molecule in gold and silver dimers. Bottom-right: Raman spectra of horseradish peroxidase (HRP) protein in a gap of 1.21 nm (small) and a gap of 2.53 nm (large) between AuNPs. Adapted with permission.^[124] Copyright 2021, American Chemical Society.

single-molecule SERS. Since there was only a single layer of origami sheet holding the AuNPs, variation of the structure from dimer to dimer was inevitable. This resulted in the observation of some of the bands of the fluorophore in question to be more pronounced in some dimers than the others. The same group also mixed this structure with graphene to reduce the fluorescence and background signal during SERS measurements.^[121] Apart from spherical NPs, Tanwar et al. decorated a rectangular origami with gold nanostar dimers.^[122] A single Texas Red dye molecule was immobilized in the hotspot between the nanostars as the Raman reporter molecule. The interparticle distance was varied between 7 and 13 nm. Enhancement factors

of 2×10^{10} and 8×10^9 were obtained for 7 and 13 nm gaps, respectively. Zhan et al. fabricated a bowtie antenna by utilizing a rectangular origami template to precisely locate two Au nanoprisms (side length of 80 nm) to form an apex-to-apex configuration with a 5 nm gap in between as given in Figure 3d.^[123] Single Cy5 or Cy3 dye molecules were separately captured in the hotspots as Raman reporters. A mean enhancement factor of 2.6×10^9 was achieved for Cy5. Polarization-dependent Raman scattering enhancement was also investigated and maximum Raman peaks were observed when excitation orientation matched the dimer axis. For the first time, the Raman spectrum of a single alkyne group was measured thanks to the

high enhancement factor provided by this bowtie geometry. Recently, Tapio et al. designed chemically specific, label-free DNA origami nanofork antennas (DONA) to optically detect single molecules and single proteins.^[124] DONA frame was a twin fork DNA origami bridged by two DNA duplexes to capture single target analytes at the hotspot as illustrated in Figure 3e. 60 nm gold and silver homodimers were connected to both arms and the gap between the particles was minimized using the zipper configuration. For larger analytes, the gap was extended by addition of three extra nucleotides to the coating strands. In the hotspot, TAMRA, Cy3.5, Cy5 dye molecules and cytochrome *c* (*cyt c*) and HRP proteins were captured before hybridizing with nanoparticles. Even in nonresonant conditions, in the small gap (1.17 nm), the Raman spectra of the dye molecules and *cyt c* could be detected. Based on the finite difference time domain simulations, such plasmonic nanoparticle dimers have signal enhancements greater than 10^9 enabling the single-molecule detection. However, when HRP protein was immobilized in the small gap, it only partially filled the hotspot and the gap stretched to 1.21 nm. Therefore, only part of HRP generated a detectable single-molecule SERS spectrum. When HRP was placed in the dimer with a larger gap, the gap stretched from 1.4 to 2.53 nm. Increasing the gap size surely helped to accommodate the HRP protein fully but no clear SERS spectrum could be observed since the signal enhancement drastically dropped with the increasing gap size.

The majority of SERS substrates are built on planar surfaces. Nevertheless, it is possible to fabricate SERS substrates on tips and use them in scanning configurations. Lately, Moeinian et al. demonstrated a silicon nanowire-based SERS substrate decorated with a DNA origami-based SERS probe for minimally invasive applications.^[125]

2.3. Directional and Polarized Emission

Another fundamental property of plasmonic antennas is their ability to control the emission pattern of quantum emitters. When an emitter is coupled to a directional antenna, the probability of finding an emitted photon at a certain solid angle is modified by the antenna mode.^[150,151] One of the most straightforward implementations of directional antennas at optical

frequencies is the phased array antennas, including the famous and prominent Yagi-Uda nanoantenna.^[41,46,150,152–155] In this multielement design, high directionality is obtained by exciting the feed element that induces the resonance of other antenna components. The coherent interference between the emission from different elements is constructive in a certain direction and destructive in the rest of the directions.^[152] Although, Yagi-Uda antennas work in a rather narrowband, log-periodic,^[156] and tapered^[157] designs provide broadband directionality.^[44] It is also possible to obtain directionality by interfering higher-order multipolar electric and magnetic modes with the dipolar mode of a single component antenna.^[158–160] In combination with field enhancement and lifetime reduction, the ability to route the emission promises directional, brighter, and faster single-photon sources,^[130] and more efficient wireless optical communication schemes.^[161]

Hübner et al. reported the bidirectional emission from a single dye molecule coupled to a DNA origami-assembled dimer antenna.^[126] A two-layered rectangular origami was used to hold two ultrasmooth 60 nm AuNPs on opposing sides of the origami. At the center of the origami, a single Cy5 dye molecule was embedded in a gap of 13 nm as shown in Figure 4a. Fluorescence lifetime measurements showed a decrease in the lifetime of Cy5 from 1.7 to 0.2 ns when incorporated into the dimer. The directionality of emission was determined by wide-field defocused imaging that gives access to the angular emission pattern of emitters. All the measurements were performed in the buffer and the fluorophore was free to rotate at a speed faster than the image acquisition time. Far-field emission patterns of dipole sources for different orientations on a substrate were simulated. A single, free-to-rotate dye standing on a substrate exhibited a radially symmetric emission pattern, whereas, an in-plane dipole showed two lobes in the emission. On the defocused images, it was observed that the dye coupled to the antenna exhibited a dipolar emission pattern, which is a signature of a dimer antenna emission, as displayed in the leftmost panel in Figure 4a.

In the same way, the polarization state of the emission of a quantum emitter that is in the vicinity of a metallic nanoparticle is determined by the plasmon mode.^[162–166] Multiple nanoparticles in different spatial configurations enable tailoring of the polarization state of emission from a single emitter.^[163,167] Quantum dots,^[168] fluorescent molecules,^[169] nitrogen-vacancy

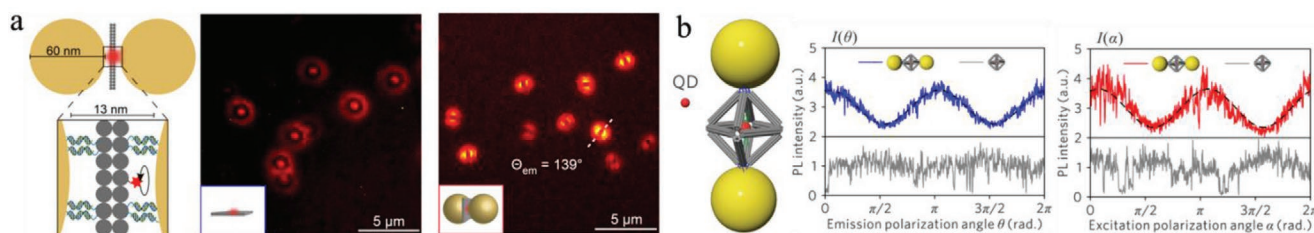


Figure 4. Directional and polarized emissions from quantum emitters placed at the hotspot of DNA origami-assisted plasmonic nanoantennas. a) A 60 nm AuNP dimer held by a rectangular origami provides a 13 nm gap and hosts a free rotating Cy5 molecule. Rotating dipole on origami results in a radially symmetric defocused image (middle panel). Two-lobed emission pattern of a dye coupled to the dimer antenna (right panel). Adapted with permission.^[126] Copyright 2019, American Chemical Society. b) Nanocluster with 50 nm AuNPs. The distance between the quantum dot center and AuNP surface is ≈ 32 nm. Plasmon-induced emission polarization of a cluster with and without AuNPs when a linear polarizer in the detection pathway is rotated with a frequency of $1/\pi \text{ rad}^{-1}$ (middle panel). Excitation polarization-dependent photoluminescence when a linear polarizer at the excitation pathway is rotated with a frequency of $1/\pi \text{ rad}^{-1}$ (right panel). Adapted with permission.^[127] Copyright 2019, American Chemical Society.

centers,^[170] and doped nanoparticles^[165] are shown to have a modified polarization determined by the antenna. Gap size is an important parameter to control the scattering polarization. In decreasing the gap size from a few to subnanometer, the polarization state of the scattered light can transit from a highly linear to unpolarized.^[171] Strongly polarized light is important as it can be used in novel displays,^[172,173] light-emitting devices,^[174] and in quantum computing, where the information is encoded as the polarization state of indistinguishable photons.^[175,176] Zhang et al. fabricated a 3D DNA origami cluster to manipulate the emission polarization of a free-floating single quantum dot.^[127] An octahedral DNA frame of six-helix bundles was designed in a way that the internal space and external connections of the frames could be utilized by site-specific DNA encoding to accommodate a single 6 nm CdSe@ZnS core-shell nanocrystal inside and AuNPs of various sizes outside of the cage. By biotin-streptavidin hybridization, the quantum dot was immobilized by eight capture strands in four in-plane edges of the origami cage. Two opposite vertices, each with four staples, were used to immobilize two 50 nm AuNPs as displayed in Figure 4b. The distance between the quantum dot center and AuNP surface was determined by small-angle X-ray scattering measurements and was ≈ 32 nm. Single-molecule confocal microscopy and fluorescence-lifetime imaging microscopy were used to investigate the polarization characteristics of the antenna. Plasmon-induced emission polarization and excitation polarization-dependent photoluminescence from the quantum dot were collected. In both cases, emission profiles were fitted with a sine function with the frequency equal to the rotation frequency of the linear polarizer in the detection and excitation optical paths, respectively. Thus, the 2D degenerate transition dipole of the nanocrystal was modified by the dimer antenna and the photoluminescence of the quantum dot became linearly polarized along the long axis of the antenna. The nanocluster is a demonstration of a polarized single-emitter light source that is not bound to any surface and can be put on other substrates, for instance with the help of a scanning probe.

3. Challenges and Opportunities

DNA origami-enabled bottom-up fabrication techniques provide easier access to build and improve the capabilities of hybrid plasmonic structures to manipulate quantum emitters' emission properties. With DNA origami-assisted plasmonic nanoantennas, unprecedented fluorescence signal enhancements and single-molecule SERS sensitivity have been demonstrated. Controlling the emission direction and polarization of a quantum emitter, and reaching the strong coupling regime are at their early development stages. Although countless opportunities lie ahead, there are still many challenges waiting to be tackled.

Even though, DNA origami offers any conceivable geometry in 2D and 3D, the area or the available volume offered by the origami is determined by the length of the used scaffold. Most origami nanobreadboards scrutinized in this review were obtained by folding single scaffolds. To scale up the nanobreadboard size and to build more complex plasmonic nanoantennas, DNA origami tiles, which are concatenated

individual origamis^[177] or longer scaffolds^[178] can be used. Shape and rigidity control of higher-order origami structures can be obtained by efficient computer simulations enabling more realistic actualization of more complex breadboards.^[179]

Noble metals,^[101–110,112,115–127] organic dyes,^[101–103,105,107,110,112,115–124,126] semiconductor nanocrystals,^[127] graphene,^[121] light-harvesting molecules,^[108] the genetic material of pathogens^[104,109] and proteins^[108,124] have been used in the construction of hybrid plasmonic antennas thanks to the available bioconjugation chemistries and site-specific functionalization of DNA origami. As the main constituent of optical antennas, there are still many uninvestigated materials that can be used as the scattering elements of DNA origami-assembled optical antennas. The palette of metallic nanoparticles constituting the plasmonic antennas has not gone beyond all-Au, all-Ag, or Au-Ag core-shell assemblies yet. Janus-like Ag-Au heterodimers fabricated by DNA origami showed that hybridized plasmon modes of heterostructures can be used to break the symmetry in coupled plasmon modes.^[180] Different species such as palladium and aluminum can be used to utilize the uncovered parts of the electromagnetic spectrum, for example, the ultraviolet regime. Unlike the fluorescence of quantum dots and dye molecules, the photoluminescence of metals does not bleach and blink. However, in the optical frequency regime, due to absorption, metals become very lossy. To address the issue of loss, it has been shown that all-dielectric nanoparticles as Mie-resonators can be used as optical antennas.^[181,182] With new functionalization protocols, all-dielectric nanoparticles can be potentially exploited as low-loss DNA origami-assisted scatterers.

Gold and silver nanoparticles are the most commonly used scattering materials so far. Even though they have been used in various shapes (spheres, rods, prisms, and nanostars) and their conjugation methods are well established, it is still a challenge to functionalize big nanoparticles as negatively charged metal is not stable in salty environments that are indispensable for the survival of the DNA origami. Spheres are the most ubiquitously used nanoparticles and the largest spherical AuNPs stably conjugated with short DNA sequences are 150 nm in diameter.^[183] For silver, the biggest spherical nanoparticle functionalized with DNA has a diameter of 100 nm.^[109] Bigger metallic nanoparticles are known to have bigger absorption and scattering cross-sections.^[184] Therefore, with bigger nanoparticles, plasmonic effects can be increased and smaller interparticle distances can be obtained with the same anchoring points. One way to make bigger nanoparticles more stable in salty buffers is to use longer DNA sequences. However, longer ones increase the gap size between nanoparticles. Another alternative is to grow the already immobilized particles on origami.^[115,116,120] However, this can lead to reduced surface smoothness and increased inhomogeneity of size distribution. Another commonly used nanoparticle shape in DNA origami-mediated plasmonic constructs is nanorods. Nanorods have anisotropic shapes that support different plasmonic modes at different wavelengths and may offer more possibilities of optical response than spheres. However, the conjugation of bigger nanorods is also a challenge. To the best of our knowledge, so far, the largest nanorods used for DNA origami-assisted plasmonic constructs has a length of about 50 nm.^[80,92]

When addressing the stability of colloidal metals, one should not omit that DNA as a biological material also needs rather strictly regulated environments, where temperature and ionic balance are the main control parameters.^[185,186] Once immobilized and dried on substrates, origami-assembled plasmonic structures bond with the surface molecules via van der Waals and Coulomb interactions and become stable without undergoing any degradation in the shape.^[187,188] However, in solution, additional stabilization processes are required. Liu et al. coated DNA origamis adsorbed on substrates with silica that provided additional rigidity to structures while maintaining their stability.^[189] They also decorated the silica-coated origamis with functionalized AuNRs. Nguyen et al. recently showed that coating the DNA origami structures with an ultrathin layer of silica prevents the origamis from degradation and aggregation in otherwise lethal ionic solvents.^[190,191] However, it was not clear if the structures were functional or modifiable after the coating. Alternatively, Gerling et al. showed that at elevated temperatures and in ultrapure water, welding the thymidine groups by ultraviolet light creates additional covalent bonds that enhance the structural stability of origamis.^[192] These covalent bonds can be cleaved afterwards.^[193] This method allows the decoration of the origami with nanoparticles or quantum emitters after the stabilization process.

The effect of the cavity on the quantum emitter's emission properties has been greatly addressed so far. However, an equally important factor in the efficient coupling of an emitter to a plasmonic antenna is the orientation of its emission dipole with respect to the main antenna mode.^[194] Having full control of the dye orientation in the cavity is critical for emission and absorption enhancements. Until now, it is still very challenging to control the relative translational and rotational motion of a dye molecule at will. Since dyes rotate faster than typical measurement durations, the obtained emission reveals an averaged result of emitter-antenna coupling under various dipole orientations. The relative motion of dye molecules in DNA origami is very much dependent on the molecular structure, attachment chemistry, and electrostatic interactions with its ultralocal environment.^[195] When a dye molecule is attached at the end of a staple constituting the origami and protrudes from it, it is difficult to control its instantaneous orientation. Recently, Mathur et al. investigated the motion and rotation of a Cy3 dye molecule in a cylindrical DNA origami bundle by placing it in different positions in the bundle with different attachment chemistries.^[196] They reported longer rotational anisotropy decay by utilizing time-resolved fluorescence anisotropy and concluded that the DNA bundle constrained the rotational motion of Cy3. Acuna and co-workers studied the effect of the nanoenvironment on relative orientations of Atto647N, Atto 643, and Cy5 dye molecules covalently attached to DNA origami.^[197] They used polarization-resolved excitation measurement to determine the orientation of absorption transition dipoles and DNA points accumulation for imaging in nanoscale topography to find out the orientation of the origamis that the dyes were incorporated into. Three scenarios were applied. In the first scenario, the fluorophores were attached at the terminus of a staple and two nucleotides from the neighboring staple were removed. In the second one, the dye molecules were again at the end of a staple but no nucleotide was removed from the

neighboring staple. In the final scenario, the dyes were attached to a position within a staple. It was observed that regardless of the type of the fluorophore, the dye molecules exhibited a stronger binding and a narrower distribution of preferred orientations in the first scenario. Molecular dynamics simulations of these three cases showed that the local environment affects the interaction of the dye with the DNA and the preferred orientation of the transition dipole. There is no doubt that further research into DNA origami-assisted manipulation of dipole orientation of quantum emitters will enable us to obtain the most efficient emission from them.

Allowed by the available bioconjugation chemistries, any organic and inorganic material can be incorporated into origami with less than 5 nm positioning resolution. This precision and addressability provided by DNA origami have been used in two ways to decorate origamis and obtain hotspots. It was either that the nanoparticles were captured by anchor groups protruding from origami with a designed nominal gap between the groups or the origami nanobreadboards were used as spacers between nanoparticles. Whichever method is preferred, gap sizes smaller than that is obtained with top-down methods can be easily achieved. The ability to obtain smaller gaps opens the doors for new applications in the following areas. Small hotspots might result in a tremendous increase in field enhancement and confinement, which increases the likelihood of detecting a single molecule in a highly concentrated biological matrix, like human blood. This bypasses the need for costly, state-of-the-art optical setups and components.^[109] The high specificity of DNA enables the target probe interaction to be utilized in sensing and diagnostic schemes. Ochmann et al.^[104] and Trofymchuk et al.^[109] demonstrated that these detectors were highly selective. In both works, when the target DNA was misplaced with two or more nucleotides, the target could not bind to the anchors in the hotspot and did not result in a fluorescence signal. Also, both DNA and gold nanoparticles are compatible with biological conditions that enable DNA origami-assisted nanoantennas to find usage in real-life medical sensing applications.

The advantages of obtaining small gaps can be utilized in further SERS applications with higher sensitivity and specificity. The tininess of DNA origami-enabled hotspots is yet to be utilized in nonlinear optical signal generation.^[198] Generation of second or higher-order harmonic signals, four-wave mixing with origami-assembled plasmonic nanoantennas hasn't been demonstrated yet. Precise control over the nanoparticle positions and tighter hotspots result in a more confined and stronger electric field, providing access to higher-order material susceptibility.^[26] Decorating an origami with different metallic particles can also help to break the symmetry of the structures. Even further reducing the gap size down to the subnanometer scale allows the quantum effects like electron tunneling and quantum nonlocal screening to be observed.^[199] These antennas might be suitable testbeds for the practical realization of quantum mechanical theories.^[200] Most hotspots elaborated so far worked in the weak coupling regime, in which the energy levels of the matter are not changed and the emission property of the emitter was modified by the antennas.^[131] Whereas, in the strong coupling regime, the cavity and the emitter hybridize and become a new quantum object. Strong

coupling can be facilitated with smaller gaps as it decreases the effective cavity volume.^[141] The strongly coupled hybrid states are of great application potential for high-speed quantum information systems.^[201]

To date, DNA origami-assisted plasmonic antenna research clustered around their sensing and spectroscopic applications. However, the ability to control the emission polarization, direction, and phase is yet to be further explored and exploited. Polarized nanoemitters in ensemble might find use in novel displays^[172,173] or light-emitting devices.^[174] Many directional plasmonic antennas have been fabricated by top-down methods.^[41,152,153,155,158–160] Design versatility offered by DNA origami can pave the way for novel single- and multielement directional antennas. For multielement antennas, each scattering component can be driven from its near-field by individual quantum emitters since DNA origami enables the precise positioning of multiple quantum emitters. DNA origami-assisted plasmonic antennas with frequency-selective directionality can be used as nanospectrometers and color routers.^[41] Optical antennas, just like their RF counterparts,^[41] can be used in wireless optical energy transfer schemes^[202,203] provided that they are directional. Multiple DNA origami-assembled directional antennas can be used to transmit optical signals from one location to another on a photonic network as long as antennas are correctly oriented with respect to each other on the substrate hosting the network. When immobilized on ordinary substrates, one major technical challenge is to align the orientation of billions of identical copies of DNA origami-assembled nanostructures. Gopinath et al. showed that it is possible to use different surface functionalization techniques to control the position and orientation of origamis on planar surfaces.^[68,204–206] New protocols can be developed to decorate origamis with nanoparticles after they are adsorbed on the functionalized surfaces to exhibit the desired plasmonic responses. Furthermore, these nanoantennas can be used as building blocks of metasurfaces to achieve tailor-made optical responses.^[20] All these modular plasmonic nanostructures can potentially be integrated into optical chips and contribute to minimization due to their small footprints that are on the order of a few hundreds of nanometers.

One of the most extraordinary advantages of using DNA origami to build antennas is that it gives the opportunity to dynamically control the conformation of as-built structures.^[80,87,93–96] It has been shown that a plasmonic particle^[97,98] or a reporting luminescing entity^[110] can walk on an origami platform when the appropriate environmental conditions are provided. The reversible and bidirectional walk of different entities making up the antenna offers the possibility to tune the optical response of the antenna in real-time.^[80,87,93,95–97] The tunable parameters include the operating frequency, the polarization state, and the pattern of the emission and have not been explored yet.

To conclude, DNA origami enables a wide range of geometrical arrangements of antenna components and precise placement of a single quantum emitter in the antenna's near-field, mostly in the hotspot. The hotspot properties are used to increase the spontaneous emission rate and brightness, enhance the absorption rate, control the emission polarization and direction of single quantum emitters. These single-emitter nanoantennas offer numerous possibilities in the fundamentals,

engineering, and applications of light–matter interactions. DNA origami-assembled plasmonic nanoantennas will surely keep extending the portfolio of antenna applications.

Acknowledgements

Financial support from Deutsche Forschungsgemeinschaft (HU2626/3-1 and HU2626/6-1) is gratefully acknowledged.

Open Access funding enabled and organized by Projekt DEAL.

Conflict of Interest

The authors declare no conflict of interest.

Keywords

DNA origami, fluorescence enhancement, optical nanoantenna, plasmonics, quantum emitter, surface-enhanced Raman scattering

Received: April 27, 2021

Revised: July 6, 2021

Published online: August 3, 2021

- [1] B. Choudhury, A. R. Sonde, R. M. Jha, *Terahertz Antenna Technology for Space Applications*, Springer, Singapore **2016**.
- [2] P. Biagioni, J.-S. Huang, B. Hecht, *Rep. Prog. Phys.* **2012**, *75*, 024402.
- [3] R. P. Feynman, *Eng. Sci. (Caltech)* **1960**, *23*, 22.
- [4] T. H. Taminiou, F. D. Stefani, N. F. van Hulst, *New J. Phys.* **2008**, *10*, 105005.
- [5] L. Novotny, *Phys. Today* **2011**, *64*, 47.
- [6] L. Novotny, N. van Hulst, *Nat. Photonics* **2011**, *5*, 83.
- [7] W. L. Barnes, A. Dereux, T. W. Ebbesen, *Nature* **2003**, *424*, 824.
- [8] G. Mie, *Ann. Phys.* **1908**, *330*, 377.
- [9] S. A. Maier, H. A. Atwater, *J. Appl. Phys.* **2005**, *98*, 011101.
- [10] P. Nordlander, C. Oubre, E. Prodan, K. Li, M. I. Stockman, *Nano Lett.* **2004**, *4*, 899.
- [11] G. Sun, J. B. Khurgin, *Appl. Phys. Lett.* **2010**, *97*, 263110.
- [12] G. Sun, J. B. Khurgin, *Appl. Phys. Lett.* **2011**, *98*, 113116.
- [13] N. Engheta, A. Salandrino, A. Alù, *Phys. Rev. Lett.* **2005**, *95*, 095504.
- [14] A. Alù, N. Engheta, *Phys. Rev. Lett.* **2008**, *101*, 043901.
- [15] A. Alù, N. Engheta, *Nat. Photonics* **2008**, *2*, 307.
- [16] J.-S. Huang, T. Feichtner, P. Biagioni, B. Hecht, *Nano Lett.* **2009**, *9*, 1897.
- [17] L. Novotny, *Phys. Rev. Lett.* **2007**, *98*, 266802.
- [18] J. Dorfmueller, R. Vogelgesang, W. Khunsin, C. Rockstuhl, C. Etrich, K. Kern, *Nano Lett.* **2010**, *10*, 3596.
- [19] R. Guo, M. Decker, F. Setzpfandt, X. Gai, D.-Y. Choi, R. Kiselev, A. Chipouline, I. Staude, T. Pertsch, D. N. Neshev, Y. S. Kivshar, *Sci. Adv.* **2017**, *3*, e1700007.
- [20] H.-T. Chen, A. J. Taylor, N. Yu, *Rep. Prog. Phys.* **2016**, *79*, 076401.
- [21] M. L. Brongersma, N. J. Halas, P. Nordlander, *Nat. Nanotechnol.* **2015**, *10*, 25.
- [22] G. Tagliabue, A. S. Jermyn, R. Sundaraman, A. J. Welch, J. S. DuChene, R. Pala, A. R. Davoyan, P. Narang, H. A. Atwater, *Nat. Commun.* **2018**, *9*, 3394.
- [23] S. Simoncelli, Y. Li, E. Cortés, S. A. Maier, *Nano Lett.* **2018**, *18*, 3400.
- [24] H. Chalabi, M. L. Brongersma, *Nat. Nanotechnol.* **2013**, *8*, 229.

- [25] M. W. Knight, H. Sobhani, P. Nordlander, N. J. Halas, *Science* **2011**, 332, 702.
- [26] M. Kauranen, A. V. Zayats, *Nat. Photonics* **2012**, 6, 737.
- [27] M. Celebrano, X. Wu, M. Baselli, S. Großmann, P. Biagioni, A. Locatelli, C. De Angelis, G. Cerullo, R. Osellame, B. Hecht, L. Duò, F. Ciccacci, M. Finazzi, *Nat. Nanotechnol.* **2015**, 10, 412.
- [28] B. Metzger, M. Hentschel, H. Giessen, *Nano Lett.* **2017**, 17, 1931.
- [29] M. Celebrano, A. Locatelli, L. Ghirardini, G. Pellegrini, P. Biagioni, A. Zilli, X. Wu, S. Grossmann, L. Carletti, C. De Angelis, L. Duò, B. Hecht, M. Finazzi, *Nano Lett.* **2019**, 19, 7013.
- [30] Y. Zhang, Y.-R. Zhen, O. Neumann, J. K. Day, P. Nordlander, N. J. Halas, *Nat. Commun.* **2014**, 5, 4424.
- [31] S. D. Gennaro, Y. Li, S. A. Maier, R. F. Oulton, *ACS Photonics* **2018**, 5, 3166.
- [32] M. I. Stockman, *Nat. Photonics* **2008**, 2, 327.
- [33] M. A. Noginov, G. Zhu, A. M. Belgrave, R. Bakker, V. M. Shalaev, E. E. Narimanov, S. Stout, E. Herz, T. Suteewong, U. Wiesner, *Nature* **2009**, 460, 1110.
- [34] J. Y. Suh, C. H. Kim, W. Zhou, M. D. Huntington, D. T. Co, M. R. Wasielewski, T. W. Odom, *Nano Lett.* **2012**, 12, 5769.
- [35] J. de Torres, M. Mivelle, S. B. Moparthy, H. Rigneault, N. F. Van Hulst, M. F. García-Parajó, E. Margeat, J. Wenger, *Nano Lett.* **2016**, 16, 6222.
- [36] J. Bohlen, Á. Cuartero-González, E. Pibiri, D. Ruhlandt, A. I. Fernández-Domínguez, P. Tinnefeld, G. P. Acuna, *Nanoscale* **2019**, 11, 7674.
- [37] W. Zhu, D. Wang, K. B. Crozier, *Nano Lett.* **2012**, 12, 6235.
- [38] M. Wersäll, R. Verre, M. Svedendahl, P. Johansson, M. Käll, T. Shegai, *J. Phys. Chem. C* **2014**, 118, 21075.
- [39] T. Shegai, P. Johansson, C. Langhammer, M. Käll, *Nano Lett.* **2012**, 12, 2464.
- [40] T. Shegai, S. Chen, V. D. Miljković, G. Zengin, P. Johansson, M. Käll, *Nat. Commun.* **2011**, 2, 481.
- [41] K.-M. See, F.-C. Lin, T.-Y. Chen, Y.-X. Huang, C.-H. Huang, A. T. M. Yesilyurt, J.-S. Huang, *Nano Lett.* **2018**, 18, 6002.
- [42] Y. Chen, *Microelectron. Eng.* **2015**, 135, 57.
- [43] J.-S. Huang, V. Callegari, P. Geisler, C. Brüning, J. Kern, J. C. Prangmsma, X. Wu, T. Feichtner, J. Ziegler, P. Weinmann, M. Kamp, A. Forchel, P. Biagioni, U. Sennhauser, B. Hecht, *Nat. Commun.* **2010**, 1, 150.
- [44] K.-P. Chen, V. P. Drachev, J. D. Borneman, A. V. Kildishev, V. M. Shalaev, *Nano Lett.* **2010**, 10, 916.
- [45] M. Pfeiffer, P. Atkinson, A. Rastelli, O. G. Schmidt, H. Giessen, M. Lippitz, K. Lindfors, *Sci. Rep.* **2018**, 8, 3415.
- [46] A. G. Curto, G. Volpe, T. H. Taminiu, M. P. Kreuzer, R. Quidant, N. F. van Hulst, *Science* **2010**, 329, 930.
- [47] E. Winfree, F. Liu, L. A. Wenzler, N. C. Seeman, *Nature* **1998**, 394, 539.
- [48] B. Shen, V. Linko, K. Tapio, S. Pikker, T. Lemma, A. Gopinath, K. V. Gothelf, M. A. Kostianen, J. J. Toppari, *Sci. Adv.* **2018**, 4, eaap8978.
- [49] P. Piskunen, B. Shen, A. Keller, J. J. Toppari, M. A. Kostianen, V. Linko, *ACS Appl. Nano Mater.* **2021**, 4, 529.
- [50] P. W. K. Rothemund, *Nature* **2006**, 440, 297.
- [51] F. Hong, F. Zhang, Y. Liu, H. Yan, *Chem. Rev.* **2017**, 117, 12584.
- [52] J. F. Marko, *1 - DNA Mechanics*, Academic Press, Boston **2018**.
- [53] B. Shen, M. A. Kostianen, V. Linko, *Langmuir* **2018**, 34, 14911.
- [54] N. Liu, T. Liedl, *Chem. Rev.* **2018**, 118, 3032.
- [55] A. Kuzyk, R. Jungmann, G. P. Acuna, N. Liu, *ACS Photonics* **2018**, 5, 1151.
- [56] H. Bui, S. A. Díaz, J. Fontana, M. Chiriboga, R. Veneziano, I. L. Medintz, *Adv. Opt. Mater.* **2019**, 7, 1900562.
- [57] K. Tapio, I. Bald, *Multifunct. Mater.* **2020**, 3, 032001.
- [58] N. Liu, *Nano Lett.* **2020**, 20, 8430.
- [59] M. Dass, F. N. Gür, K. Kořataj, M. J. Urban, T. Liedl, *J. Phys. Chem. C* **2021**, 125, 5969.
- [60] N. Maccaferri, G. Barbillon, A. N. Koya, G. Lu, G. P. Acuna, D. Garoli, *Nanoscale Adv.* **2021**, 3, 633.
- [61] C. A. Mirkin, R. L. Letsinger, R. C. Mucic, J. J. Storhoff, *Nature* **1996**, 382, 607.
- [62] A. P. Alivisatos, K. P. Johnsson, X. Peng, T. E. Wilson, C. J. Loweth, M. P. Bruchez, P. G. Schultz, *Nature* **1996**, 382, 609.
- [63] B. Liu, J. Liu, *Anal. Methods* **2017**, 9, 2633.
- [64] B. Liu, J. Liu, *Langmuir* **2019**, 35, 6476.
- [65] a) B. Liu, T. Wu, Z. Huang, Y. Liu, J. Liu, *Angew. Chem.* **2019**, 131, 2131; b) B. Liu, T. Wu, Z. Huang, Y. Liu, J. Liu, *Angew. Chem., Int. Ed.* **2019**, 58, 2109.
- [66] B. Liu, J. Liu, *Matter* **2019**, 1, 825.
- [67] J. J. Funke, H. Dietz, *Nat. Nanotechnol.* **2016**, 11, 47.
- [68] A. Xu, J. N. Harb, M. A. Kostianen, W. L. Hughes, A. T. Woolley, H. Liu, A. Gopinath, *MRS Bull.* **2017**, 42, 943.
- [69] B. Ding, Z. Deng, H. Yan, S. Cabrini, R. N. Zuckermann, J. Bokor, *J. Am. Chem. Soc.* **2010**, 132, 3248.
- [70] S. Pal, Z. Deng, H. Wang, S. Zou, Y. Liu, H. Yan, *J. Am. Chem. Soc.* **2011**, 133, 17606.
- [71] F. N. Gür, F. W. Schwarz, J. Ye, S. Diez, T. L. Schmidt, *ACS Nano* **2016**, 10, 5374.
- [72] a) C. Steinhauer, R. Jungmann, T. L. Sobey, F. C. Simmel, P. Tinnefeld, *Angew. Chem.* **2009**, 121, 9030; b) C. Steinhauer, R. Jungmann, T. L. Sobey, F. C. Simmel, P. Tinnefeld, *Angew. Chem., Int. Ed.* **2009**, 48, 8870.
- [73] I. H. Stein, C. Steinhauer, P. Tinnefeld, *J. Am. Chem. Soc.* **2011**, 133, 4193.
- [74] R. Schreiber, J. Do, E.-M. Roller, T. Zhang, V. J. Schüller, P. C. Nickels, J. Feldmann, T. Liedl, *Nat. Nanotechnol.* **2014**, 9, 74.
- [75] F. N. Gür, C. P. T. McPolin, S. Raza, M. Mayer, D. J. Roth, A. M. Steiner, M. Löffler, A. Fery, M. L. Brongersma, A. V. Zayats, T. A. F. König, T. L. Schmidt, *Nano Lett.* **2018**, 18, 7323.
- [76] a) C. Heck, Y. Kanehira, J. Kneipp, I. Bald, *Angew. Chem.* **2018**, 130, 7566; b) C. Heck, Y. Kanehira, J. Kneipp, I. Bald, *Angew. Chem., Int. Ed.* **2018**, 57, 7444.
- [77] F. Praetorius, B. Kick, K. L. Behler, M. N. Honemann, D. Weuster-Botz, H. Dietz, *Nature* **2017**, 552, 84.
- [78] R. Schreiber, I. Santiago, A. Ardavan, A. J. Turberfield, *ACS Nano* **2016**, 10, 7303.
- [79] M. J. Urban, P. K. Dutta, P. Wang, X. Duan, X. Shen, B. Ding, Y. Ke, N. Liu, *J. Am. Chem. Soc.* **2016**, 138, 5495.
- [80] A. Kuzyk, M. J. Urban, A. Idili, F. Ricci, N. Liu, *Sci. Adv.* **2017**, 3, e1602803.
- [81] W. Fang, S. Jia, J. Chao, L. Wang, X. Duan, H. Liu, Q. Li, X. Zuo, L. Wang, L. Wang, N. Liu, C. Fan, *Sci. Adv.* **2019**, 5, eaau4506.
- [82] C. Zhou, Y. Yang, H. Li, F. Gao, C. Song, D. Yang, F. Xu, N. Liu, Y. Ke, S. Su, P. Wang, *Nano Lett.* **2020**, 20, 3155.
- [83] C. Heck, J. Prinz, A. Dathe, V. Merk, O. Straniik, W. Fritzsche, J. Kneipp, I. Bald, *ACS Photonics* **2017**, 4, 1123.
- [84] K. Voegelé, J. List, G. Pardatscher, N. B. Holland, F. C. Simmel, T. Pirzer, *ACS Nano* **2016**, 10, 11377.
- [85] A. Kuzyk, R. Schreiber, Z. Fan, G. Pardatscher, E.-M. Roller, A. Högele, F. C. Simmel, A. O. Govorov, T. Liedl, *Nature* **2012**, 483, 311.
- [86] C. Zhou, X. Duan, N. Liu, *Acc. Chem. Res.* **2017**, 50, 2906.
- [87] X. Lan, T. Liu, Z. Wang, A. O. Govorov, H. Yan, Y. Liu, *J. Am. Chem. Soc.* **2018**, 140, 11763.
- [88] N. Aissaoui, K. Moth-Poulsen, M. Käll, P. Johansson, L. M. Wilhelmsson, B. Albinsson, *Nanoscale* **2017**, 9, 673.
- [89] E.-M. Roller, L. V. Besteiro, C. Pupp, L. K. Khorashad, A. O. Govorov, T. Liedl, *Nat. Phys.* **2017**, 13, 761.
- [90] I. Kaminska, J. Bohlen, S. Rocchetti, F. Selbach, G. P. Acuna, P. Tinnefeld, *Nano Lett.* **2019**, 19, 4257.

- [91] J. Schnitzbauer, M. T. Strauss, T. Schlichthaerle, F. Schueder, R. Jungmann, *Nat. Protoc.* **2017**, *12*, 1198.
- [92] L. M. Kneer, E.-M. Roller, L. V. Besteiro, R. Schreiber, A. O. Govorov, T. Liedl, *ACS Nano* **2018**, *12*, 9110.
- [93] C. Zhou, L. Xin, X. Duan, M. J. Urban, N. Liu, *Nano Lett.* **2018**, *18*, 7395.
- [94] Q. Jiang, Q. Liu, Y. Shi, Z.-G. Wang, P. Zhan, J. Liu, C. Liu, H. Wang, X. Shi, L. Zhang, J. Sun, B. Ding, M. Liu, *Nano Lett.* **2017**, *17*, 7125.
- [95] P. Zhan, P. K. Dutta, P. Wang, G. Song, M. Dai, S.-X. Zhao, Z.-G. Wang, P. Yin, W. Zhang, B. Ding, Y. Ke, *ACS Nano* **2017**, *11*, 1172.
- [96] L. Xin, C. Zhou, X. Duan, N. Liu, *Nat. Commun.* **2019**, *10*, 5394.
- [97] C. Zhou, X. Duan, N. Liu, *Nat. Commun.* **2015**, *6*, 8102.
- [98] M. J. Urban, C. Zhou, X. Duan, N. Liu, *Nano Lett.* **2015**, *15*, 8392.
- [99] M. Madsen, K. V. Gothelf, *Chem. Rev.* **2019**, *119*, 6384.
- [100] S. Dey, C. Fan, K. V. Gothelf, J. Li, C. Lin, L. Liu, N. Liu, M. A. D. Nijenhuis, B. Saccà, F. C. Simmel, H. Yan, P. Zhan, *Nat. Rev. Methods Primers* **2021**, *1*, 13.
- [101] G. P. Acuna, F. M. Möller, P. Holzmeister, S. Beater, B. Lalkens, P. Tinnefeld, *Science* **2012**, *338*, 506.
- [102] A. Puchkova, C. Vietz, E. Pibiri, B. Wünsch, M. Sanz Paz, G. P. Acuna, P. Tinnefeld, *Nano Lett.* **2015**, *15*, 8354.
- [103] T. Zhang, N. Gao, S. Li, M. J. Lang, Q.-H. Xu, *J. Phys. Chem. Lett.* **2015**, *6*, 2043.
- [104] S. E. Ochmann, C. Vietz, K. Trofymchuk, G. P. Acuna, B. Lalkens, P. Tinnefeld, *Anal. Chem.* **2017**, *89*, 13000.
- [105] C. Vietz, B. Lalkens, G. P. Acuna, P. Tinnefeld, *Nano Lett.* **2017**, *17*, 6496.
- [106] C. Vietz, I. Kaminska, M. Sanz Paz, P. Tinnefeld, G. P. Acuna, *ACS Nano* **2017**, *11*, 4969.
- [107] I. Kaminska, C. Vietz, Á. Cuartero-González, P. Tinnefeld, A. I. Fernández-Domínguez, G. P. Acuna, *Nanophotonics* **2018**, *7*, 643.
- [108] I. Kaminska, J. Bohlen, S. Mackowski, P. Tinnefeld, G. P. Acuna, *ACS Nano* **2018**, *12*, 1650.
- [109] K. Trofymchuk, V. Glembockyte, L. Grabenhorst, F. Steiner, C. Vietz, C. Close, M. Pfeiffer, L. Richter, M. L. Schütte, F. Selbach, R. Yaadav, J. Zähringer, Q. Wei, A. Ozcan, B. Lalkens, G. P. Acuna, P. Tinnefeld, *Nat. Commun.* **2021**, *12*, 950.
- [110] L. Xin, M. Lu, S. Both, M. Pfeiffer, M. J. Urban, C. Zhou, H. Yan, T. Weiss, N. Liu, K. Lindfors, *ACS Photonics* **2019**, *6*, 985.
- [111] E.-M. Roller, C. Argyropoulos, A. Högele, T. Liedl, M. Pilo-Pais, *Nano Lett.* **2016**, *16*, 5962.
- [112] R. Chikkaraddy, V. A. Turek, N. Kongsuwan, F. Benz, C. Carnegie, T. van de Goor, B. de Nijs, A. Demetriadou, O. Hess, U. F. Keyser, J. J. Baumberg, *Nano Lett.* **2018**, *18*, 405.
- [113] O. S. Ojambati, R. Chikkaraddy, W. D. Deacon, M. Horton, D. Kos, V. A. Turek, U. F. Keyser, J. J. Baumberg, *Nat. Commun.* **2019**, *10*, 1049.
- [114] J. Zhu, F. Wu, Z. Han, Y. Shang, F. Liu, H. Yu, L. Yu, N. Li, B. Ding, *Nano Lett.* **2021**, *21*, 3573.
- [115] J. Prinz, B. Schreiber, L. Olejko, J. Oertel, J. Rackwitz, A. Keller, I. Bald, *J. Phys. Chem. Lett.* **2013**, *4*, 4140.
- [116] M. Pilo-Pais, A. Watson, S. Demers, T. H. LaBean, G. Finkelstein, *Nano Lett.* **2014**, *14*, 2099.
- [117] V. V. Thacker, L. O. Herrmann, D. O. Sigle, T. Zhang, T. Liedl, J. J. Baumberg, U. F. Keyser, *Nat. Commun.* **2014**, *5*, 3448.
- [118] P. Kühler, E.-M. Roller, R. Schreiber, T. Liedl, T. Lohmüller, J. Feldmann, *Nano Lett.* **2014**, *14*, 2914.
- [119] S. Simoncelli, E.-M. Roller, P. Urban, R. Schreiber, A. J. Turberfield, T. Liedl, T. Lohmüller, *ACS Nano* **2016**, *10*, 9809.
- [120] J. Prinz, C. Heck, L. Ellerik, V. Merk, I. Bald, *Nanoscale* **2016**, *8*, 5612.
- [121] J. Prinz, A. Matković, J. Pešić, R. Gajić, I. Bald, *Small* **2016**, *12*, 5458.
- [122] S. Tanwar, K. K. Haldar, T. Sen, *J. Am. Chem. Soc.* **2017**, *139*, 17639.
- [123] a) P. Zhan, T. Wen, Z.-g. Wang, Y. He, J. Shi, T. Wang, X. Liu, G. Lu, B. Ding, *Angew. Chem.* **2018**, *130*, 2896; b) P. Zhan, T. Wen, Z.-g. Wang, Y. He, J. Shi, T. Wang, X. Liu, G. Lu, B. Ding, *Angew. Chem., Int. Ed.* **2018**, *57*, 2846.
- [124] K. Tapio, A. Mostafa, Y. Kanehira, A. Suma, A. Dutta, I. Bald, *ACS Nano* **2021**, *15*, 7065.
- [125] A. Moeinian, F. N. Gür, J. Gonzalez-Torres, L. Zhou, V. D. Murugesan, A. D. Dashtestani, H. Guo, T. L. Schmidt, S. Strehle, *Nano Lett.* **2019**, *19*, 1061.
- [126] K. Hübner, M. Pilo-Pais, F. Selbach, T. Liedl, P. Tinnefeld, F. D. Stefani, G. P. Acuna, *Nano Lett.* **2019**, *19*, 6629.
- [127] H. Zhang, M. Li, K. Wang, Y. Tian, J.-S. Chen, K. T. Fountaine, D. DiMarzio, M. Liu, M. Cotlet, O. Gang, *ACS Nano* **2020**, *14*, 1369.
- [128] E. M. Purcell, *Phys. Rev.* **1946**, *69*, 674.
- [129] P. Törmä, W. L. Barnes, *Rep. Prog. Phys.* **2014**, *78*, 013901.
- [130] A. F. Koenderink, *ACS Photonics* **2017**, *4*, 710.
- [131] J. T. Hugall, A. Singh, N. F. van Hulst, *ACS Photonics* **2018**, *5*, 43.
- [132] P. J. Schuck, D. P. Fromm, A. Sundaramurthy, G. S. Kino, W. E. Moerner, *Phys. Rev. Lett.* **2005**, *94*, 017402.
- [133] L. V. Besteiro, X.-T. Kong, Z. Wang, G. Hartland, A. O. Govorov, *ACS Photonics* **2017**, *4*, 2759.
- [134] B. Gallinet, O. J. F. Martin, *ACS Nano* **2011**, *5*, 8999.
- [135] T. B. Hoang, G. M. Akselrod, C. Argyropoulos, J. Huang, D. R. Smith, M. H. Mikkelsen, *Nat. Commun.* **2015**, *6*, 7788.
- [136] A. Kinkhabwala, Z. Yu, S. Fan, Y. Avlasevich, K. Müllen, W. E. Moerner, *Nat. Photonics* **2009**, *3*, 654.
- [137] G. M. Akselrod, C. Argyropoulos, T. B. Hoang, C. Ciraci, C. Fang, J. Huang, D. R. Smith, M. H. Mikkelsen, *Nat. Photonics* **2014**, *8*, 835.
- [138] L. Y. M. Tobing, D. H. Zhang, K. E. Fong, M. D. Birowosuto, Y. Gao, C. Dang, H. V. Demir, *ACS Photonics* **2018**, *5*, 1566.
- [139] S. I. Bogdanov, M. Y. Shalaginov, A. S. Lagutchev, C.-C. Chiang, D. Shah, A. S. Baburin, I. A. Ryzhikov, I. A. Rodionov, A. V. Kildishev, A. Boltasseva, V. M. Shalae, *Nano Lett.* **2018**, *18*, 4837.
- [140] M. Pfeiffer, K. Lindfors, H. Zhang, B. Fenk, F. Philipp, P. Atkinson, A. Rastelli, O. G. Schmidt, H. Giessen, M. Lippitz, *Nano Lett.* **2014**, *14*, 197.
- [141] R. Chikkaraddy, B. de Nijs, F. Benz, S. J. Barrow, O. A. Scherman, E. Rosta, A. Demetriadou, P. Fox, O. Hess, J. J. Baumberg, *Nature* **2016**, *535*, 127.
- [142] P. K. Jain, D. Ghosh, R. Baer, E. Rabani, A. P. Alivisatos, *Proc. Natl. Acad. Sci. USA* **2012**, *109*, 8016.
- [143] N. Rivera, I. Kaminer, B. Zhen, J. D. Joannopoulos, M. Soljačić, *Science* **2016**, *353*, 263.
- [144] J. Langer, D. Jimenez de Aberasturi, J. Aizpurua, R. A. Alvarez-Puebla, B. Auguie, J. J. Baumberg, G. C. Bazan, S. E. J. Bell, A. Boisen, A. G. Brolo, J. Choo, D. Cialla-May, V. Deckert, L. Fabris, K. Faulds, F. J. García de Abajo, R. Goodacre, D. Graham, A. J. Haes, C. L. Haynes, C. Huck, T. Itoh, M. Käll, J. Kneipp, N. A. Kotov, H. Kuang, E. C. Le Ru, H. K. Lee, J.-F. Li, X. Y. Ling, S. A. Maier, T. Mayerhöfer, M. Moskovits, K. Murakoshi, J.-M. Nam, S. Nie, Y. Ozaki, I. Pastoriza-Santos, J. Perez-Juste, J. Popp, A. Pucci, S. Reich, B. Ren, G. C. Schatz, T. Shegai, S. Schlücker, L.-L. Tay, K. G. Thomas, Z.-Q. Tian, R. P. Van Duyne, T. Vo-Dinh, Y. Wang, K. A. Willets, C. Xu, H. Xu, Y. Xu, Y. S. Yamamoto, B. Zhao, L. M. Liz-Marzán, *ACS Nano* **2020**, *14*, 28.
- [145] E. C. Le Ru, E. Blackie, M. Meyer, P. G. Etchegoin, *J. Phys. Chem. C* **2007**, *111*, 13794.
- [146] S. L. Kleinman, B. Sharma, M. G. Blaber, A.-I. Henry, N. Valley, R. G. Freeman, M. J. Natan, G. C. Schatz, R. P. Van Duyne, *J. Am. Chem. Soc.* **2013**, *135*, 301.
- [147] a) S. Schlücker, *Angew. Chem.* **2014**, *126*, 4852; b) S. Schlücker, *Angew. Chem., Int. Ed.* **2014**, *53*, 4756.
- [148] S. Yang, X. Dai, B. B. Stogin, T.-S. Wong, *Proc. Natl. Acad. Sci. USA* **2016**, *113*, 268.

- [149] K. Kneipp, Y. Wang, H. Kneipp, L. T. Perelman, I. Itzkan, R. R. Dasari, M. S. Feld, *Phys. Rev. Lett.* **1997**, *78*, 1667.
- [150] T. H. Taminiau, F. D. Stefani, N. F. van Hulst, *Opt. Express* **2008**, *16*, 10858.
- [151] T. H. Taminiau, F. D. Stefani, F. B. Segerink, N. F. van Hulst, *Nat. Photonics* **2008**, *2*, 234.
- [152] T. Kosako, Y. Kadoya, H. F. Hofmann, *Nat. Photonics* **2010**, *4*, 312.
- [153] D. Dregely, R. Taubert, J. Dorfmueller, R. Vogelgesang, K. Kern, H. Giessen, *Nat. Commun.* **2011**, *2*, 267.
- [154] I. S. Maksymov, I. Staude, A. E. Miroshnichenko, Y. S. Kivshar, *Nanophotonics* **2012**, *1*, 65.
- [155] M. Ramezani, A. Casadei, G. Grzela, F. Matteini, G. Tütüncüoğlu, D. Ruffer, A. Fontcuberta i Morral, J. G. Rivas, *Nano Lett.* **2015**, *15*, 4889.
- [156] R. S. Pavlov, A. G. Curto, N. F. van Hulst, *Opt. Commun.* **2012**, *285*, 3334.
- [157] I. S. Maksymov, A. R. Davoyan, Y. S. Kivshar, *Appl. Phys. Lett.* **2011**, *99*, 083304.
- [158] A. G. Curto, T. H. Taminiau, G. Volpe, M. P. Kreuzer, R. Quidant, N. F. van Hulst, *Nat. Commun.* **2013**, *4*, 1750.
- [159] D. Vercrucy, X. Zheng, Y. Sonnefraud, N. Verellen, G. Di Martino, L. Lagae, G. A. E. Vandenbosch, V. V. Moshchalkov, S. A. Maier, P. Van Dorpe, *ACS Nano* **2014**, *8*, 8232.
- [160] I. M. Hancu, A. G. Curto, M. Castro-López, M. Kuttge, N. F. van Hulst, *Nano Lett.* **2014**, *14*, 166.
- [161] M. Cohen, Y. Abulafia, D. Lev, A. Lewis, R. Shavit, Z. Zalevsky, *Nano Lett.* **2017**, *17*, 5181.
- [162] R. J. Moerland, T. H. Taminiau, L. Novotny, N. F. van Hulst, L. Kuipers, *Nano Lett.* **2008**, *8*, 606.
- [163] T. Shegai, Z. Li, T. Dadosh, Z. Zhang, H. Xu, G. Haran, *Proc. Natl. Acad. Sci. USA* **2008**, *105*, 16448.
- [164] T. Ming, L. Zhao, Z. Yang, H. Chen, L. Sun, J. Wang, C. Yan, *Nano Lett.* **2009**, *9*, 3896.
- [165] L. Chen, Y. Rong, M. Ren, W. Wu, M. Qin, C. Pan, Q. Ma, S. Liu, B. Wu, E. Wu, J. Xu, H. Zeng, *J. Phys. Chem. C* **2018**, *122*, 15666.
- [166] T. Zuo, H. J. Goldwyn, B. P. Isaacoff, D. J. Masiello, J. S. Biteen, *J. Phys. Chem. Lett.* **2019**, *10*, 5047.
- [167] Z. Li, T. Shegai, G. Haran, H. Xu, *ACS Nano* **2009**, *3*, 637.
- [168] H. Mertens, J. S. Biteen, H. A. Atwater, A. Polman, *Nano Lett.* **2006**, *6*, 2622.
- [169] T. Ming, L. Zhao, H. Chen, K. C. Woo, J. Wang, H.-Q. Lin, *Nano Lett.* **2011**, *11*, 2296.
- [170] S. K. H. Andersen, S. Kumar, S. I. Bozhevolnyi, *Nano Lett.* **2017**, *17*, 3889.
- [171] L. Yang, H. Wang, Y. Fang, Z. Li, *ACS Nano* **2016**, *10*, 1580.
- [172] A. Montali, C. Bastiaansen, P. Smith, C. Weder, *Nature* **1998**, *392*, 261.
- [173] M. Grell, D. D. C. Bradley, *Adv. Mater.* **1999**, *11*, 895.
- [174] E. Matioli, S. Brinkley, K. M. Kelchner, Y.-L. Hu, S. Nakamura, S. DenBaars, J. Speck, C. Weisbuch, *Light: Sci. Appl.* **2012**, *1*, e22.
- [175] L. Sansoni, K. H. Luo, C. Eigner, R. Ricken, V. Quiring, H. Herrmann, C. Silberhorn, *npj Quantum Inf.* **2017**, *3*, 5.
- [176] R. Vasconcelos, S. Reisenbauer, C. Salter, G. Wachter, D. Wirtitsch, J. Schmiedmayer, P. Walther, M. Trupke, *npj Quantum Inf.* **2020**, *6*, 9.
- [177] Z. Zhao, Y. Liu, H. Yan, *Nano Lett.* **2011**, *11*, 2997.
- [178] A. N. Marchi, I. Saaem, B. N. Vogen, S. Brown, T. H. LaBean, *Nano Lett.* **2014**, *14*, 5740.
- [179] J. Y. Lee, J. G. Lee, G. Yun, C. Lee, Y.-J. Kim, K. S. Kim, T. H. Kim, D.-N. Kim, *ACS Nano* **2021**, *15*, 1002.
- [180] L. Weller, V. V. Thacker, L. O. Herrmann, E. A. Hemmig, A. Lombardi, U. F. Keyser, J. J. Baumberg, *ACS Photonics* **2016**, *3*, 1589.
- [181] A. I. Kuznetsov, A. E. Miroshnichenko, M. L. Brongersma, Y. S. Kivshar, B. Luk'yanchuk, *Science* **2016**, *354*, aag2472.
- [182] D. G. Baranov, D. A. Zuev, S. I. Lepeshov, O. V. Kotov, A. E. Krasnok, A. B. Evlyukhin, B. N. Chichkov, *Optica* **2017**, *4*, 814.
- [183] C. Vietz, B. Lalkens, G. P. Acuna, P. Tinnefeld, *New J. Phys.* **2016**, *18*, 045012.
- [184] E. A. Coronado, E. R. Encina, F. D. Stefani, *Nanoscale* **2011**, *3*, 4042.
- [185] H. Kim, S. P. Surwade, A. Powell, C. O'Donnell, H. Liu, *Chem. Mater.* **2014**, *26*, 5265.
- [186] J. A. L. Roodhuizen, P. J. T. M. Hendriks, P. A. J. Hilbers, T. F. A. de Greef, A. J. Markvoort, *ACS Nano* **2019**, *13*, 10798.
- [187] Y. Chen, P. Wang, Y. Xu, X. Li, Y. Zhu, Y. Zhang, J. Zhu, G. Huang, D. He, *ACS Appl. Bio Mater.* **2018**, *1*, 1424.
- [188] S. Ramakrishnan, H. Ijäs, V. Linko, A. Keller, *Comput. Struct. Biotechnol. J.* **2018**, *16*, 342.
- [189] X. Liu, F. Zhang, X. Jing, M. Pan, P. Liu, W. Li, B. Zhu, J. Li, H. Chen, L. Wang, J. Lin, Y. Liu, D. Zhao, H. Yan, C. Fan, *Nature* **2018**, *559*, 593.
- [190] a) L. Nguyen, M. Döblinger, T. Liedl, A. Heuer-Jungemann, *Angew. Chem.* **2019**, *131*, 924; b) L. Nguyen, M. Döblinger, T. Liedl, A. Heuer-Jungemann, *Angew. Chem., Int. Ed.* **2019**, *58*, 912.
- [191] M.-K. Nguyen, V. H. Nguyen, A. K. Natarajan, Y. Huang, J. Ryssy, B. Shen, A. Kuzyk, *Chem. Mater.* **2020**, *32*, 6657.
- [192] T. Gerling, M. Kube, B. Kick, H. Dietz, *Sci. Adv.* **2018**, *4*, eaau1157.
- [193] a) T. Gerling, H. Dietz, *Angew. Chem.* **2019**, *131*, 2706; b) T. Gerling, H. Dietz, *Angew. Chem., Int. Ed.* **2019**, *58*, 2680.
- [194] R. Carminati, A. Cazé, D. Cao, F. Peragut, V. Krachmalnicoff, R. Pierrat, Y. De Wilde, *Surf. Sci. Rep.* **2015**, *70*, 1.
- [195] J. Ouellet, S. Schorr, A. Iqbal, T. J. Wilson, D. M. J. Lilley, *Biophys. J.* **2011**, *101*, 1148.
- [196] D. Mathur, Y. C. Kim, S. A. Díaz, P. D. Cunningham, B. S. Rolczynski, M. G. Ancona, I. L. Medintz, J. S. Melinger, *J. Phys. Chem. C* **2021**, *125*, 1509.
- [197] K. Hübner, H. Joshi, A. Aksimentiev, F. D. Stefani, P. Tinnefeld, G. P. Acuna, *ACS Nano* **2021**, *15*, 5109.
- [198] M. Pilo-Pais, G. P. Acuna, P. Tinnefeld, T. Liedl, *MRS Bull.* **2017**, *42*, 936.
- [199] W. Zhu, R. Esteban, A. G. Borisov, J. J. Baumberg, P. Nordlander, H. J. Lezec, J. Aizpurua, K. B. Crozier, *Nat. Commun.* **2016**, *7*, 11495.
- [200] C. Tserkezis, A. T. M. Yeşilyurt, J.-S. Huang, N. A. Mortensen, *ACS Photonics* **2018**, *5*, 5017.
- [201] A. F. Koenderink, A. Alù, A. Polman, *Science* **2015**, *348*, 516.
- [202] D. Dregely, K. Lindfors, M. Lippitz, N. Engheta, M. Totzeck, H. Giessen, *Nat. Commun.* **2014**, *5*, 4354.
- [203] A. Dasgupta, M.-M. Mennemanteuil, M. Buret, N. Cazier, G. Colas-des-Francis, A. Bouhelier, *Nat. Commun.* **2018**, *9*, 1992.
- [204] A. Gopinath, P. W. K. Rothmund, *ACS Nano* **2014**, *8*, 12030.
- [205] A. Gopinath, E. Miyazono, A. Faraon, P. W. K. Rothmund, *Nature* **2016**, *535*, 401.
- [206] A. Gopinath, C. Thachuk, A. Mitskovets, H. A. Atwater, D. Kirkpatrick, P. W. K. Rothmund, *Science* **2021**, *371*, eabd6179.



Ayşe Tuğça Mina Yeşilyurt obtained her Bachelor of Science in Electrical and Electronics Engineering from Bilkent University, Turkey in 2010. She was granted an Erasmus Mundus scholarship and obtained the joint Master of Science in Photonics degree from Ghent University, Belgium, and the University of St Andrews, Scotland, UK, in 2012. Later, she worked at the Scientific and Technological Research Council of Turkey until 2017. Currently, she is a doctoral candidate at the Friedrich Schiller University Jena, Germany, and a member of the Research Department of Nanooptics at the Leibniz Institute of Photonic Technology. Her research interests are directional plasmonic nanoantennas and DNA origami.



Jer-Shing Huang is currently the head of the Research Department of Nanooptics at the Leibniz Institute of Photonic Technology in Jena, Germany. He is also an adjunct professor at the Department of Electrophysics at National Yang Ming Chiao Tung University and an adjunct research fellow at the Research Center for Applied Sciences of Academia Sinica in Taiwan. Before 2016, Dr. Huang was an associate professor at the Department of Chemistry at National Tsing Hua University in Taiwan. His research focuses on the engineering of nanoscale light–matter interaction using rationally designed plasmonic and dielectric nanostructures.